

NASA TECHNICAL MEMORANDUM



NASA TM X-1658

NASA TM X-1658

GPO PRICE \$ _____

CSFTI PRICE(S) \$ _____

Hard copy (HC) _____

Microfiche (MF) _____

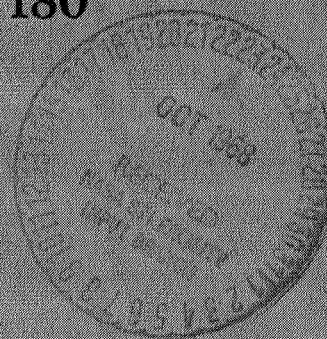
ff 653 July 65

N 68-36193

FACILITY FORM 602	(ACCESSION NUMBER)	(THRU)
	40 (PAGES)	1 (CODE)
	(NASA CR OR TMX OR AD NUMBER)	01 (CATEGORY)

AERODYNAMIC CHARACTERISTICS OF BODIES OF REVOLUTION AT MACH NUMBERS FROM 1.50 TO 2.86 AND ANGLES OF ATTACK TO 180°

by Lloyd S. Jernell
Langley Research Center
Langley Station, Hampton, Va.



AERODYNAMIC CHARACTERISTICS OF BODIES
OF REVOLUTION AT MACH NUMBERS FROM 1.50 TO 2.86
AND ANGLES OF ATTACK TO 180°

By Lloyd S. Jernell

Langley Research Center
Langley Station, Hampton, Va.

NATIONAL AERONAUTICS AND SPACE ADMINISTRATION

AERODYNAMIC CHARACTERISTICS OF BODIES
OF REVOLUTION AT MACH NUMBERS FROM 1.50 TO 2.86
AND ANGLES OF ATTACK TO 180°

By Lloyd S. Jernell
Langley Research Center

SUMMARY

An investigation has been conducted in the Langley Unitary Plan wind tunnel to determine the aerodynamic characteristics of a series of cylinder, cone-cylinder, and ogive-cylinder bodies with various nose and afterbody fineness ratios for angles of attack from 0° to 180° and Mach numbers from 1.50 to 2.86.

The data indicated that with the center of gravity located at 50 percent of the body length, none of the test configurations were statically stable at angles of attack near 0° or 180°. The magnitude of the normal force was primarily dependent upon the magnitude of the planform area. Generally, the more rearward the planform-area centroid, the more rearward the center of pressure.

INTRODUCTION

In studies of the upper atmosphere and outer space, a parachute is frequently used as a means for payload recovery. The recovery of the intact payload by this means generally requires that substantial reductions in vehicle velocity be achieved prior to parachute deployment. To insure the relatively high drag levels needed for deceleration, it is desirable that the payload be unstable so as to avoid trim conditions at low-drag orientations, such as angles of attack near 0° and 180°.

Thus, it is necessary to determine the longitudinal stability characteristics of a given payload throughout the angle-of-attack spectrum so that the center of gravity of the payload may be appropriately positioned. Since the length and shape of payloads vary considerably, a systematic study of the aerodynamic characteristics of bodies with various nose shapes and fineness ratios was deemed desirable in order to gain an insight into the variables that might affect trim conditions.

Accordingly, an investigation was initiated to determine the longitudinal aerodynamic characteristics of a series of cylinder, cone-cylinder, and ogive-cylinder bodies with various nose and afterbody fineness ratios. The investigation was performed

in the Langley Unitary Plan wind tunnel at Mach numbers from 1.50 to 2.86 throughout an angle-of-attack range from about -5° to 185° . The test Reynolds number was 1.0×10^6 per foot (3.28×10^6 per meter).

The results of an investigation of the effects of fineness ratio and nose shape on the aerodynamic characteristics of similar configurations for angles of attack to about 90° and Mach numbers from 2.37 to 3.90 are presented in reference 1.

SYMBOLS

The data are referred to the body-axis system with the moment center of each configuration located along the model center line at 50 percent of the body length.

A	model cross-sectional area
A _{plan}	model planform area
C _A	axial-force coefficient, $\frac{\text{Axial force}}{qA}$
C _m	pitching-moment coefficient, $\frac{\text{Pitching moment}}{qAd}$
C _N	normal-force coefficient, $\frac{\text{Normal force}}{qA}$
C _{N'}	normal-force coefficient based on planform area, $\frac{\text{Normal force}}{qA_{\text{plan}}}$
d	body diameter
l	total model length
l _A	length of afterbody section
l _N	length of nose section
M	free-stream Mach number
q	free-stream dynamic pressure
x _{cp}	distance of center of pressure from model nose apex

\bar{x} distance of planform-area centroid from model nose apex

α angle of attack of model center line, deg

APPARATUS AND METHODS

Models

Drawings of the models are shown in figure 1. A straight sting was used for the nominal angle-of-attack ranges from 0° to 45° and 135° to 180° . For the latter range, enough of the nose was removed to allow for sting clearance. For the angle ranges from 45° to 90° and 90° to 135° , the sting entered the model through a side cavity (shown by dashed lines in fig. 1) and had a 45° bend (enclosed by model) that aligned the end of the sting with the balance.

Tunnel

The investigation was conducted in the low Mach number test section of the Langley Unitary Plan wind tunnel, which is a variable-pressure, continuous-flow facility. The test section is 4 feet square by approximately 7 feet long. The nozzle leading to the test section is of the asymmetric, sliding-block type, which permits a continuous variation in Mach number from 1.47 to 2.86.

Measurements, Corrections, and Test Conditions

Aerodynamic forces and moments were measured by means of a sting-supported, six-component, strain-gage balance housed within the model fuselage. The axial-force coefficients presented herein represent the total axial force; that is, no adjustment was made for the model base-pressure conditions. The angles of attack were corrected for tunnel flow angularity and for the deflection of the model support system due to aerodynamic load.

The tests were conducted at Mach numbers from 1.50 to 2.86 and a Reynolds number of 1.0×10^6 per foot (3.28×10^6 per meter). The angle-of-attack range was approximately -5° to 185° . The dewpoint was maintained below -30° F to prevent significant tunnel condensation effects.

Boundary-layer transition was effected by bands of small triangular pieces of (pressure-sensitive plastic film) tape, 0.0075 inch (0.0191 cm) thick, affixed 1 inch (2.54 cm) aft of the nose apex for angles of attack from 0° to 90° and 1 inch (2.54 cm) from the base for the angle-of-attack range from 90° to 180° .

DISCUSSION

Presented in figure 2 is a sequence of schlieren photographs obtained at $M = 1.50$ showing typical shock patterns generated by the model and its support system in the regions of overlapping angle of attack; that is, at angles of attack of approximately 45° , 75° , 105° , and 135° .

Longitudinal data for the two cylindrical models with fineness ratios of 6 and 8 are presented in figure 3. An increase in fineness ratio results in an increase in normal-force coefficient at angles of attack from 0° to 90° . This increase in normal force, in turn, is reflected in a positive increment in pitching-moment coefficient at the lower Mach numbers. The difference in C_N due to an increase in fineness ratio appears to become slightly greater with increase in Mach number, whereas the effect of fineness ratio on C_m vanishes as the Mach number is increased to 2.86. For the cylinders investigated, fineness ratio has little effect on axial-force coefficient.

The effect of afterbody fineness ratio l_A/d on the longitudinal stability characteristics of the cone-cylinder models with a nose fineness ratio of 3 is shown in figure 4. An increase in afterbody fineness ratio leads to an increase in normal-force coefficient throughout the test Mach number and angle-of-attack ranges. At angles of attack to 45° , an increase in afterbody fineness ratio results in a positive increment in C_m , whereas, at angles of attack from 45° to 180° , an increase in afterbody fineness ratio leads to a negative increment in C_m . The effects of afterbody fineness ratio on the longitudinal stability characteristics of the ogive-cylinder models with a nose fineness ratio of 5 (fig. 5) are similar to those discussed for the cone-cylinder models of figure 4.

The discontinuities exhibited by the data are believed to be due primarily to interference effects of the model support system. For example, the schlieren photograph of figure 2(a), for $\alpha \approx 45^\circ$, shows the trailing shock from the model base being influenced by the flow field surrounding the sting flare. This condition would be expected to affect the axial force. With the 45° bent sting installed, figures 2(b) to 2(e) show that as the angle of attack approaches 90° the aft portion of the model comes under an increasing influence of the high-pressure field induced by the support-system flare; thus, normal force and pitch characteristics as well as axial-force characteristics are affected. As would be expected, the data indicate that the degree of influence is greater for those configurations having larger portions of the body in close proximity to the sting flare. These data indicate the need for further study of model support-system techniques for extremely high angle-of-attack testing in order to minimize these interference effects.

The effects of nose fineness ratio on the longitudinal stability characteristics of the ogive-cylinder models having an afterbody fineness ratio of 6 are shown in figure 6. An increase in nose fineness ratio results in an increase in normal-force coefficient at all test angles of attack ($0^\circ < \alpha < 180^\circ$) and at all test Mach numbers. The pitching-moment coefficient becomes more negative with increasing nose fineness ratio. This negative trend reflects, as expected, a more rearward location of the center of pressure on the models with higher nose fineness ratio.

The data of figures 3 to 6 indicate that none of the configurations having the center of gravity at 50 percent of the body length are statically stable at angles of attack near 0° or 180° .

The effects of nose shape on the longitudinal stability characteristics of the models having a nose fineness ratio of 3 and an afterbody fineness ratio of 6 are shown in figure 7. The ogive-nose configuration exhibits slightly greater values of normal-force coefficient, and less negative values of pitching-moment coefficient than does the cone-cylinder model. The effect of nose shape (cone or ogive) on axial-force coefficient is negligible.

The variation of the normal-force coefficient based on planform area C_N' with overall fineness ratio l/d is shown in figure 8 for Mach numbers of 1.50 and 2.86 and arbitrarily chosen angles of attack of 30° , 70° , 110° , and 150° . At $M = 1.50$, although a small decrease in the normal-force parameter is generally noted as fineness ratio is increased, no effect due to nose shape is discernible. At $M = 2.86$, neither fineness ratio nor nose shape has an effect on the normal-force parameter. Thus, these data indicate that the magnitude of the normal force is primarily dependent upon the magnitude of the planform area.

The variation of the center of pressure in percent of body length, x_{cp}/l , with angle of attack is presented in figures 9 to 12. All models exhibit a rapid rearward travel of the center of pressure with increasing angle of attack to approximately 20° and above approximately 160° . For the interim angles ($20^\circ \lesssim \alpha \lesssim 160^\circ$), the rate of change of the center of pressure with angle of attack is relatively low and approaches a linear variation.

The variation of center of pressure with the planform-area centroid at several angles of attack is shown in figure 13. Generally, the more rearward the planform-area centroid, the more rearward the center of pressure.

CONCLUSIONS

An investigation has been conducted in the Langley Unitary Plan wind tunnel to determine the aerodynamic characteristics of a series of cylinder, cone-cylinder, and

ogive-cylinder bodies with various nose and afterbody fineness ratios for angles of attack from 0° to 180° and Mach numbers from 1.50 to 2.86. The results of the investigation indicated the following conclusions:

1. With the center of gravity located at 50 percent of the body length, none of the test configurations were statically stable at angles of attack near 0° or 180° .
2. The magnitude of the normal force was primarily dependent upon the magnitude of the planform area.
3. Generally, the more rearward the planform-area centroid, the more rearward the center of pressure.

Langley Research Center,
National Aeronautics and Space Administration,
Langley Station, Hampton, Va., June 14, 1968,
124-07-05-01-23.

REFERENCE

1. Smith, Fred M.: A Wind-Tunnel Investigation of the Aerodynamic Characteristics of Bodies of Revolution at Mach Numbers of 2.37, 2.98, and 3.90 at Angles of Attack to 90° . NASA TM X-311, 1960.

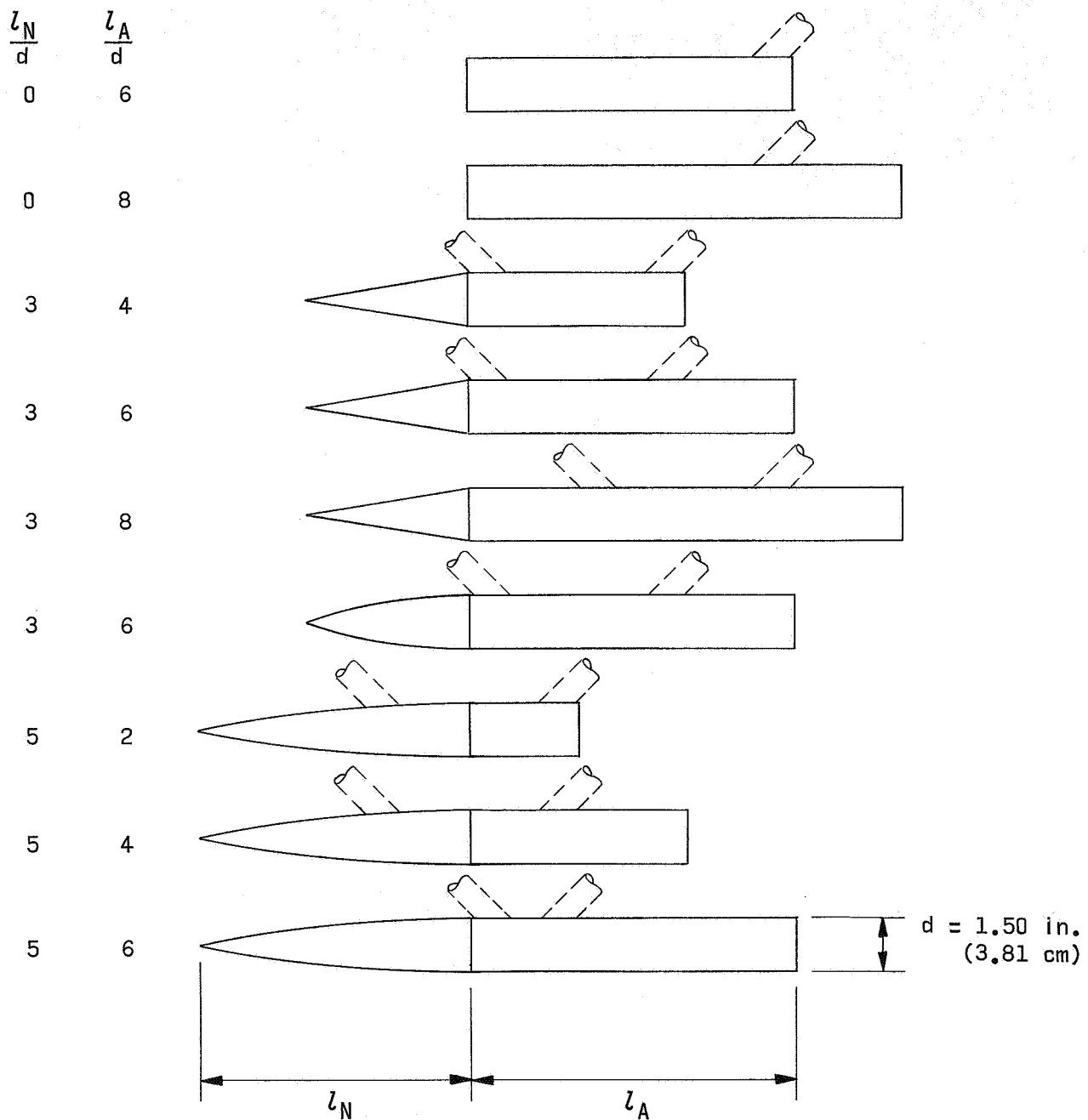
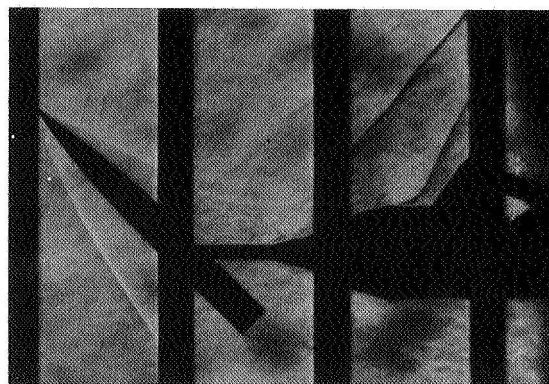


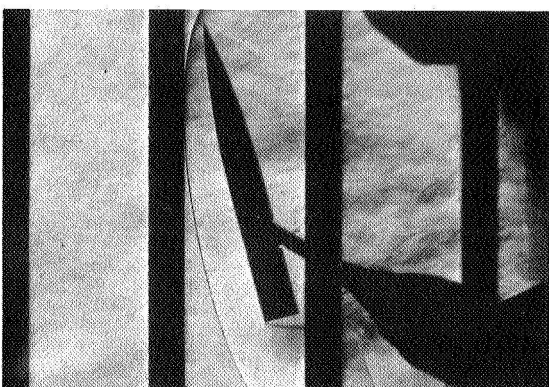
Figure 1.- Model drawings. Dashed lines indicate the various 45° bent sting arrangements.



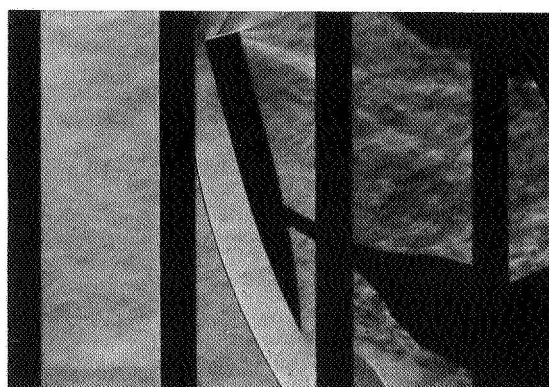
(a) Model mounting for $\alpha = 0^\circ$ to 45° , shown at $\alpha \approx 45^\circ$.



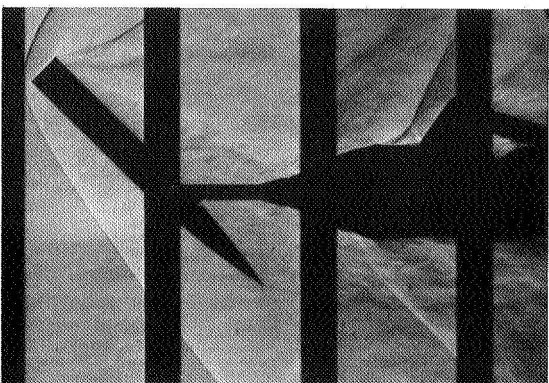
(b) Model mounting for $\alpha = 45^\circ$ to 90° , shown at $\alpha \approx 45^\circ$.



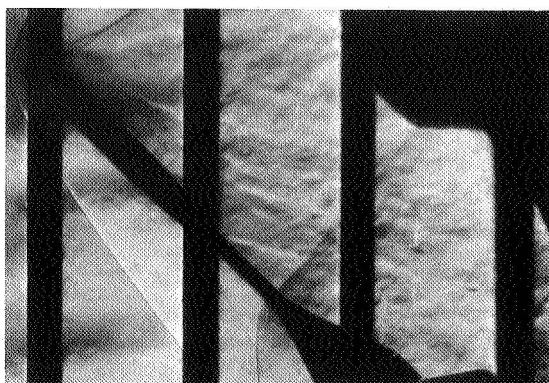
(c) Model mounting for $\alpha = 45^\circ$ to 90° , shown at $\alpha \approx 75^\circ$.



(d) Model mounting for $\alpha = 90^\circ$ to 135° , shown at $\alpha \approx 105^\circ$.

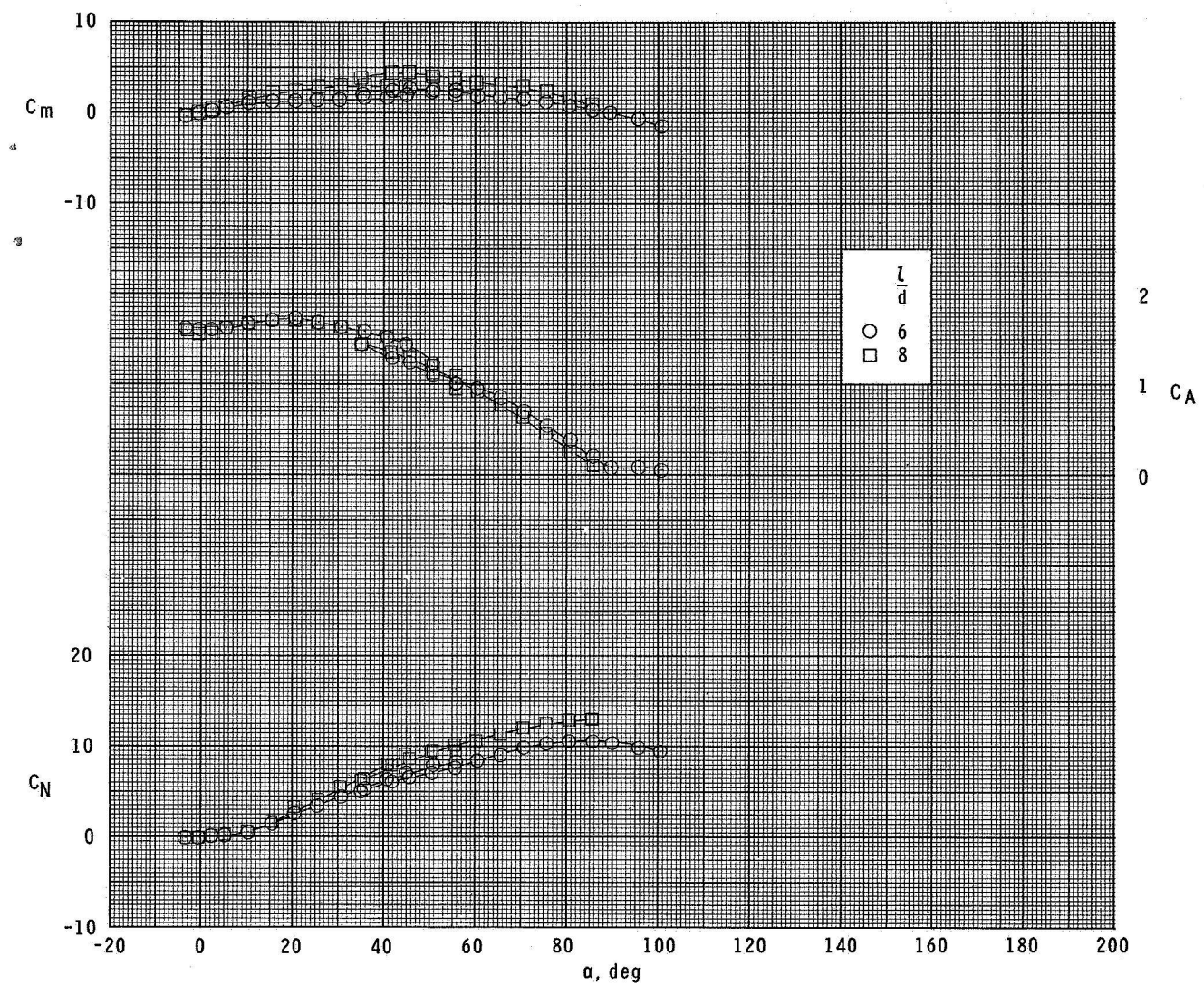


(e) Model mounting for $\alpha = 90^\circ$ to 135° , shown at $\alpha \approx 135^\circ$.



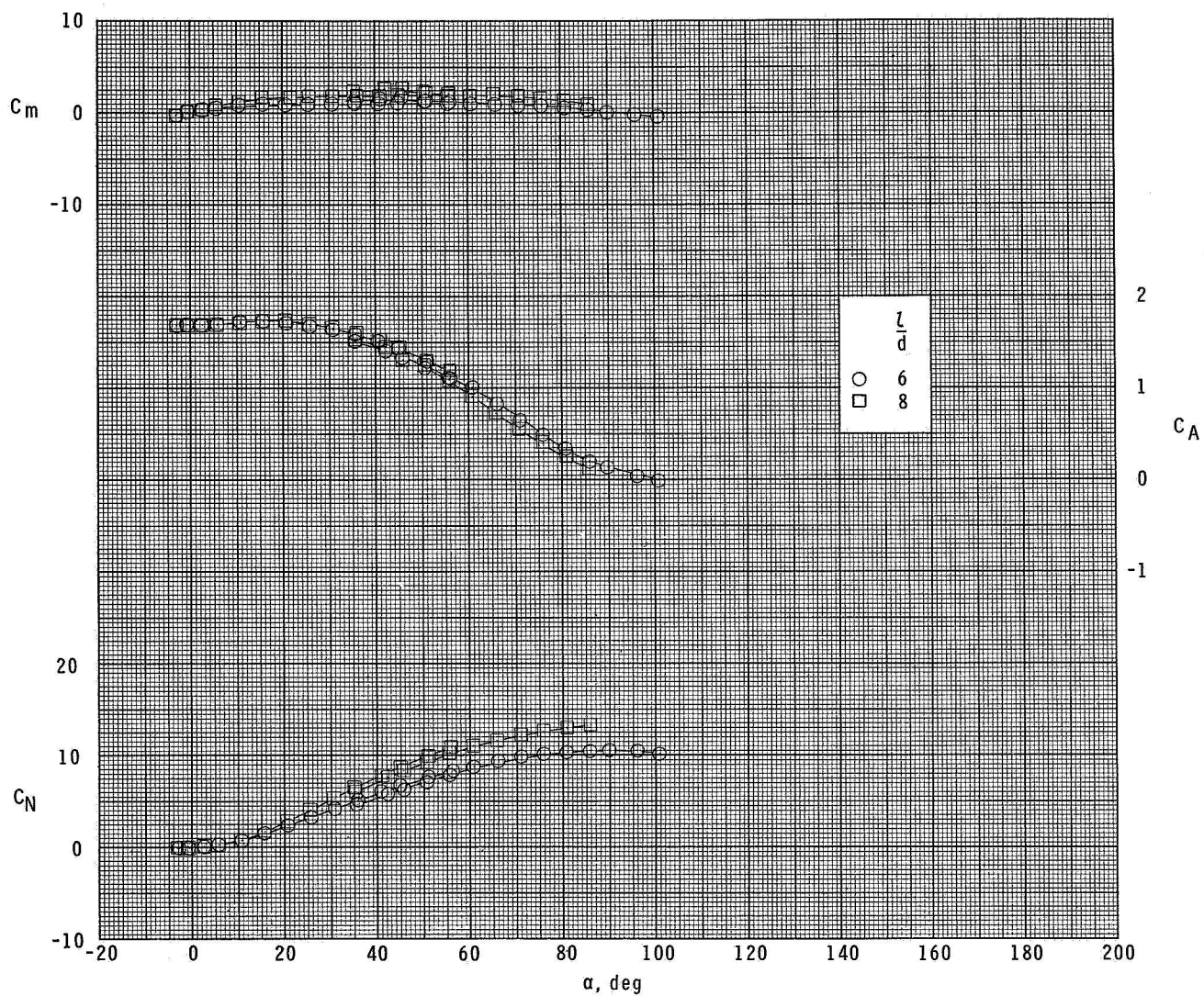
(f) Model mounting for $\alpha = 135^\circ$ to 180° , shown at $\alpha \approx 135^\circ$.
L-68-5640

Figure 2.- Schlieren photographs of ogive-cylinder model showing typical shock patterns and model mountings for the various nominal angle-of-attack ranges. $M = 1.50$; $\frac{l_N}{d} = 5$; $\frac{l_A}{d} = 4$.



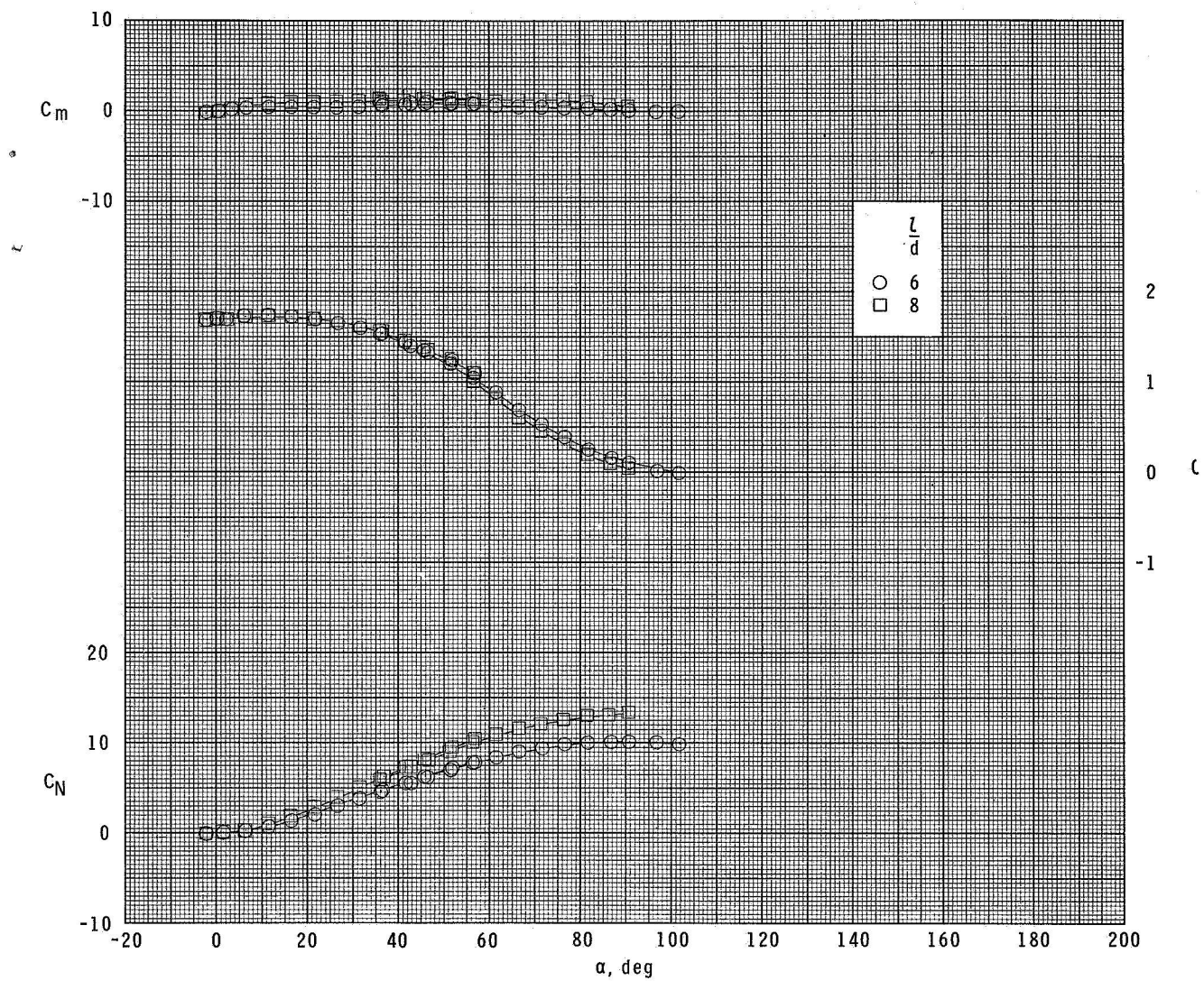
(a) $M=1.50$.

Figure 3.- Effect of fineness ratio on longitudinal stability characteristics of cylindrical models.



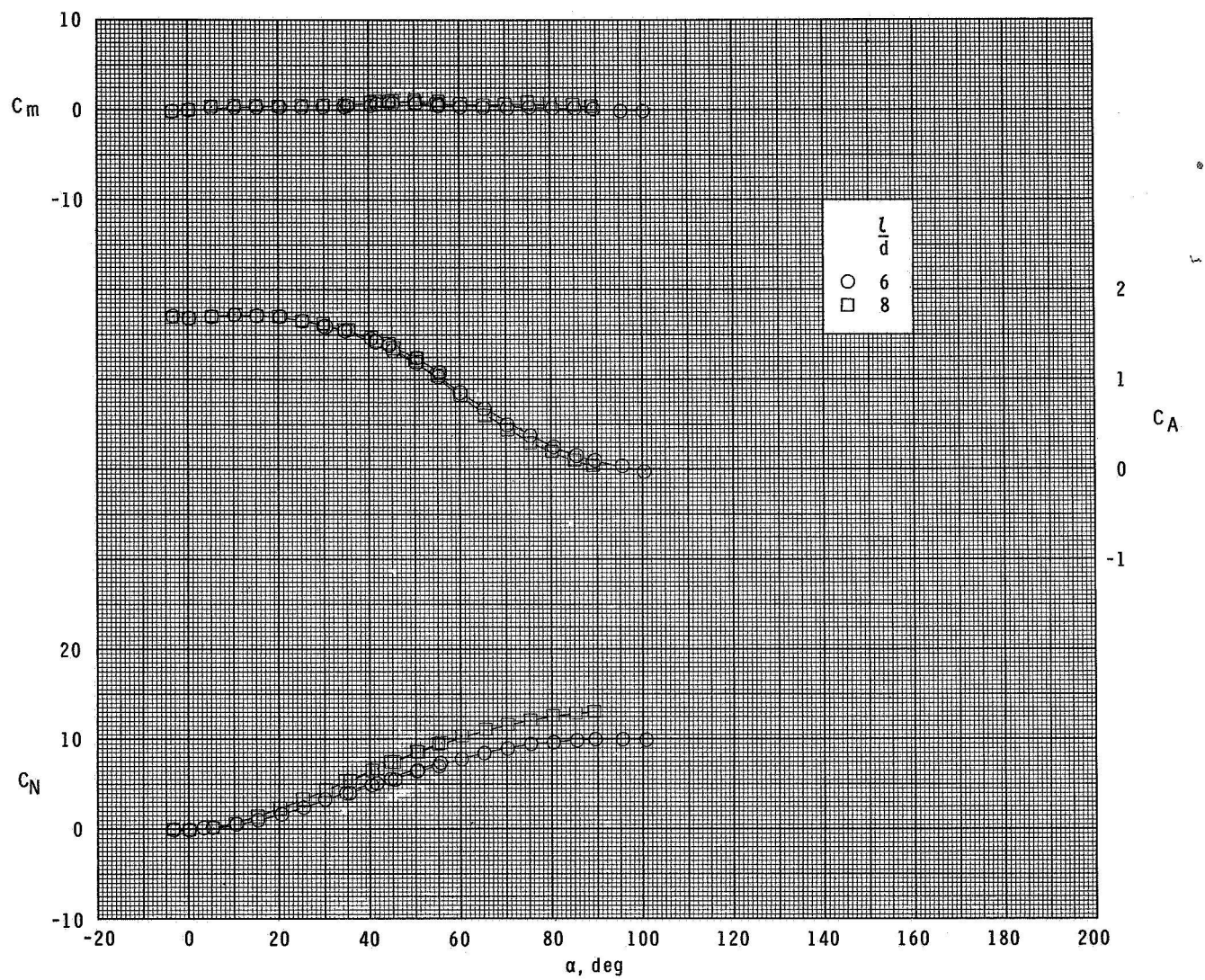
(b) $M = 1.90$.

Figure 3.- Continued.



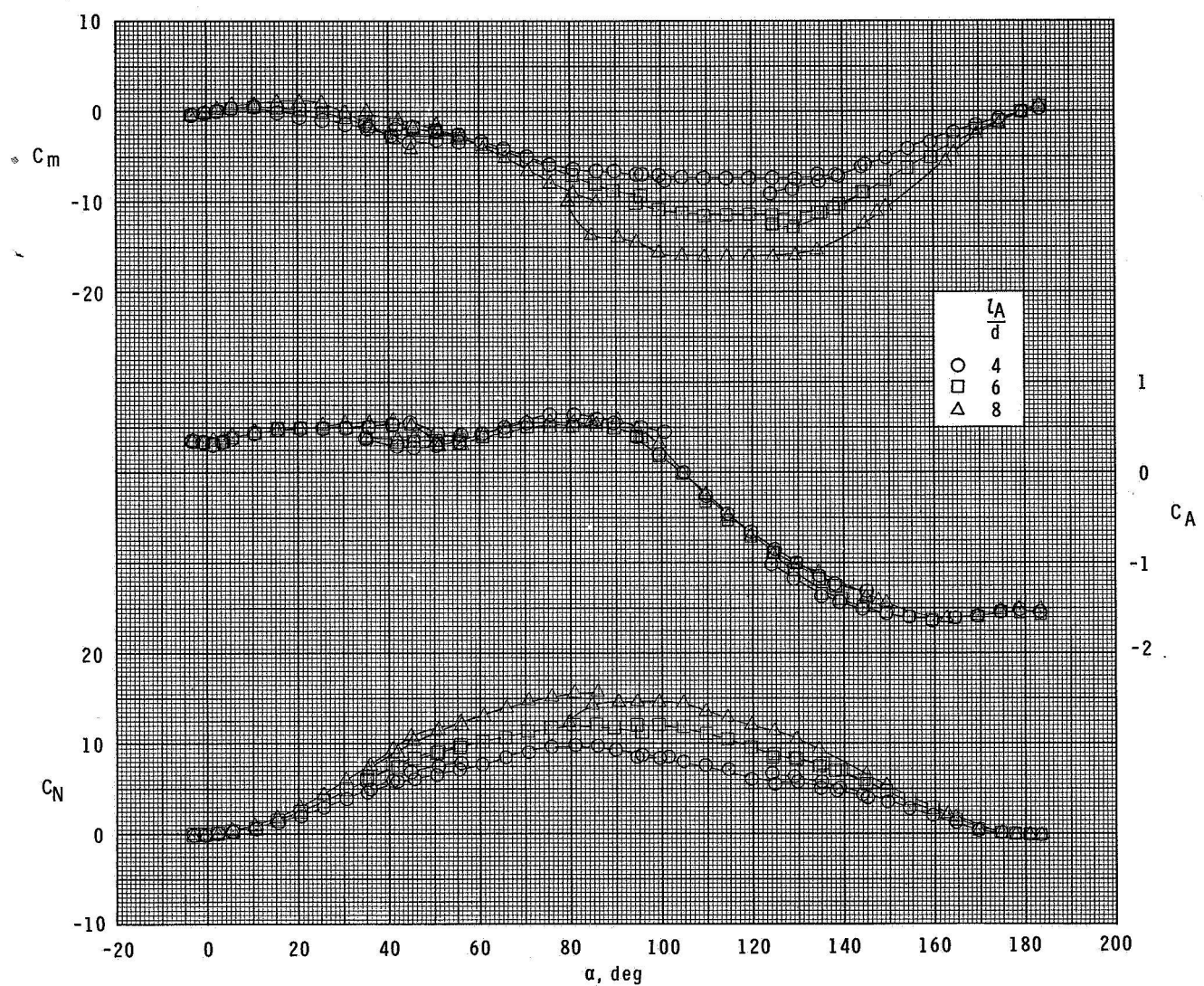
(c) $M=2.36$.

Figure 3.- Continued.



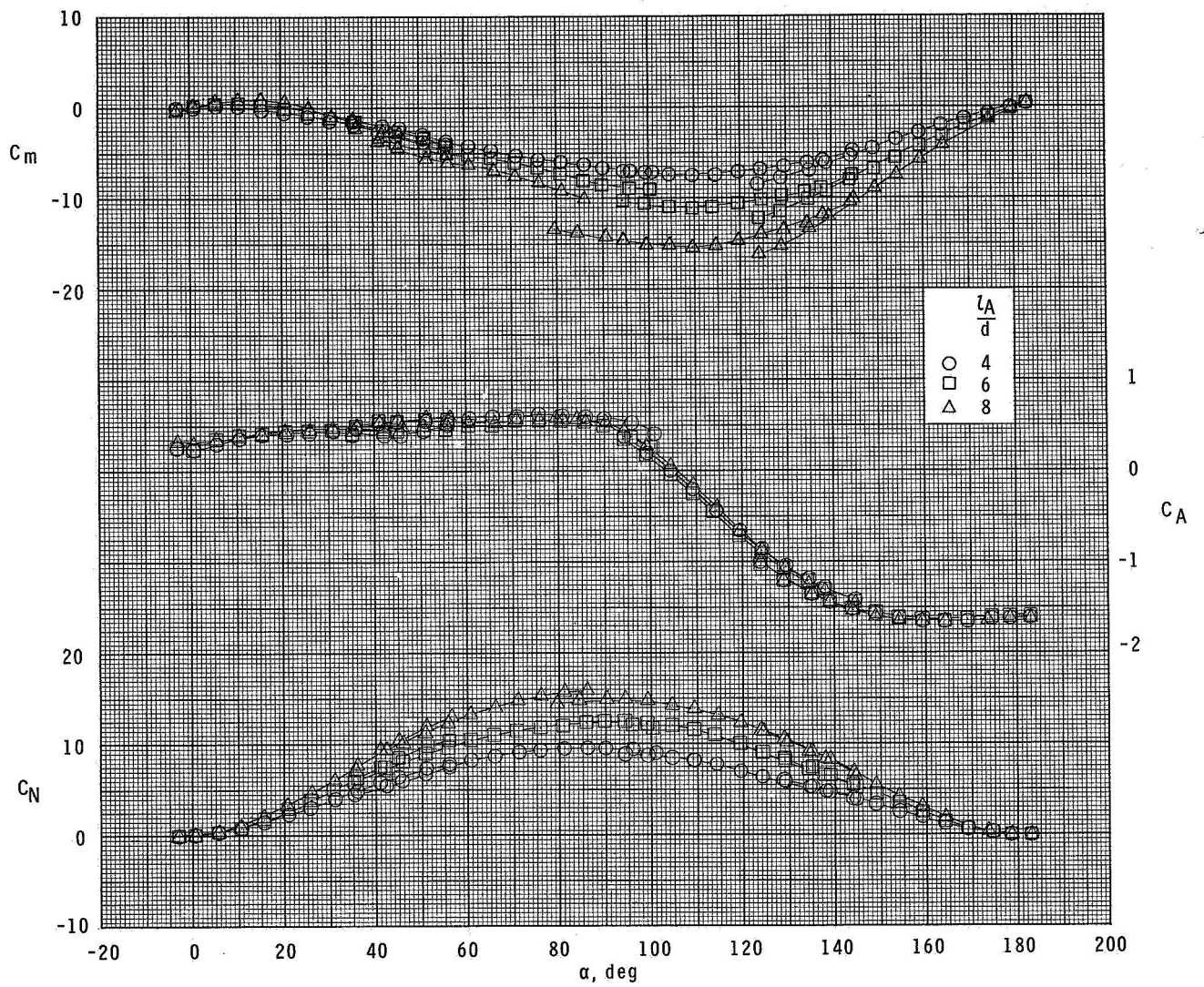
(d) $M = 2.86$.

Figure 3.- Concluded.



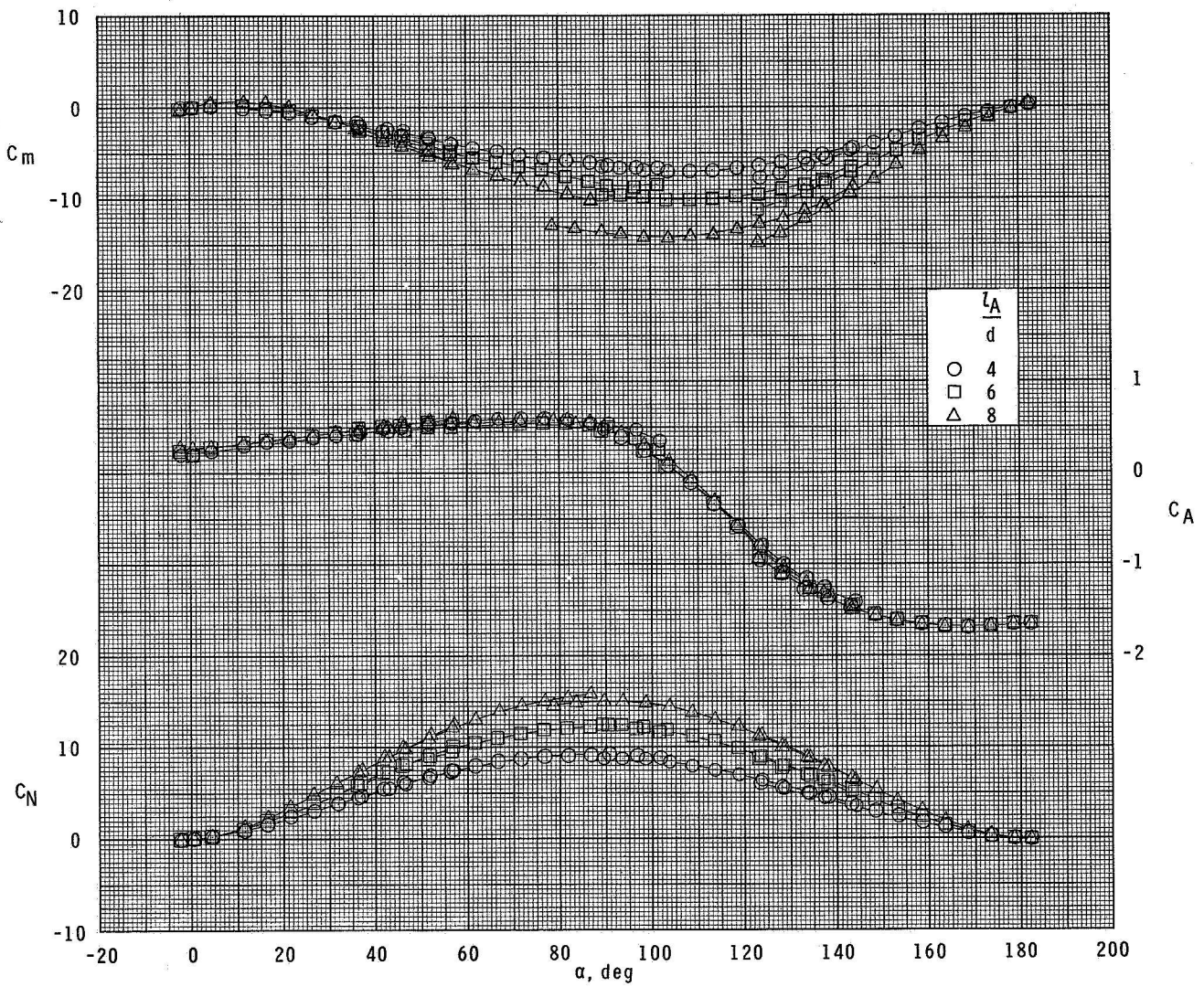
(a) $M=1.50$.

Figure 4.- Effect of afterbody fineness ratio on longitudinal stability characteristics of cone-cylinder models with nose fineness ratio of 3.



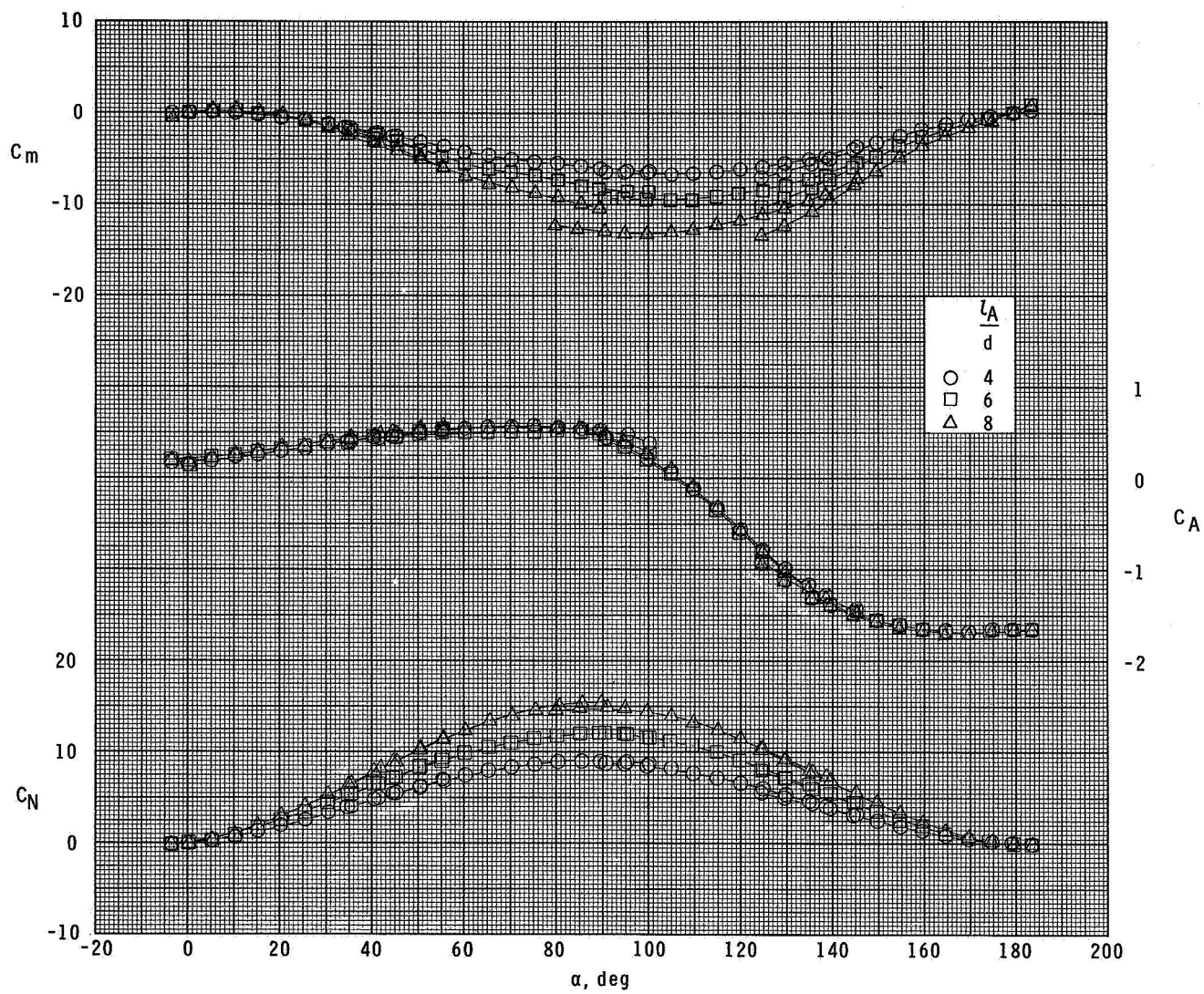
(b) $M=1.90$.

Figure 4.- Continued.



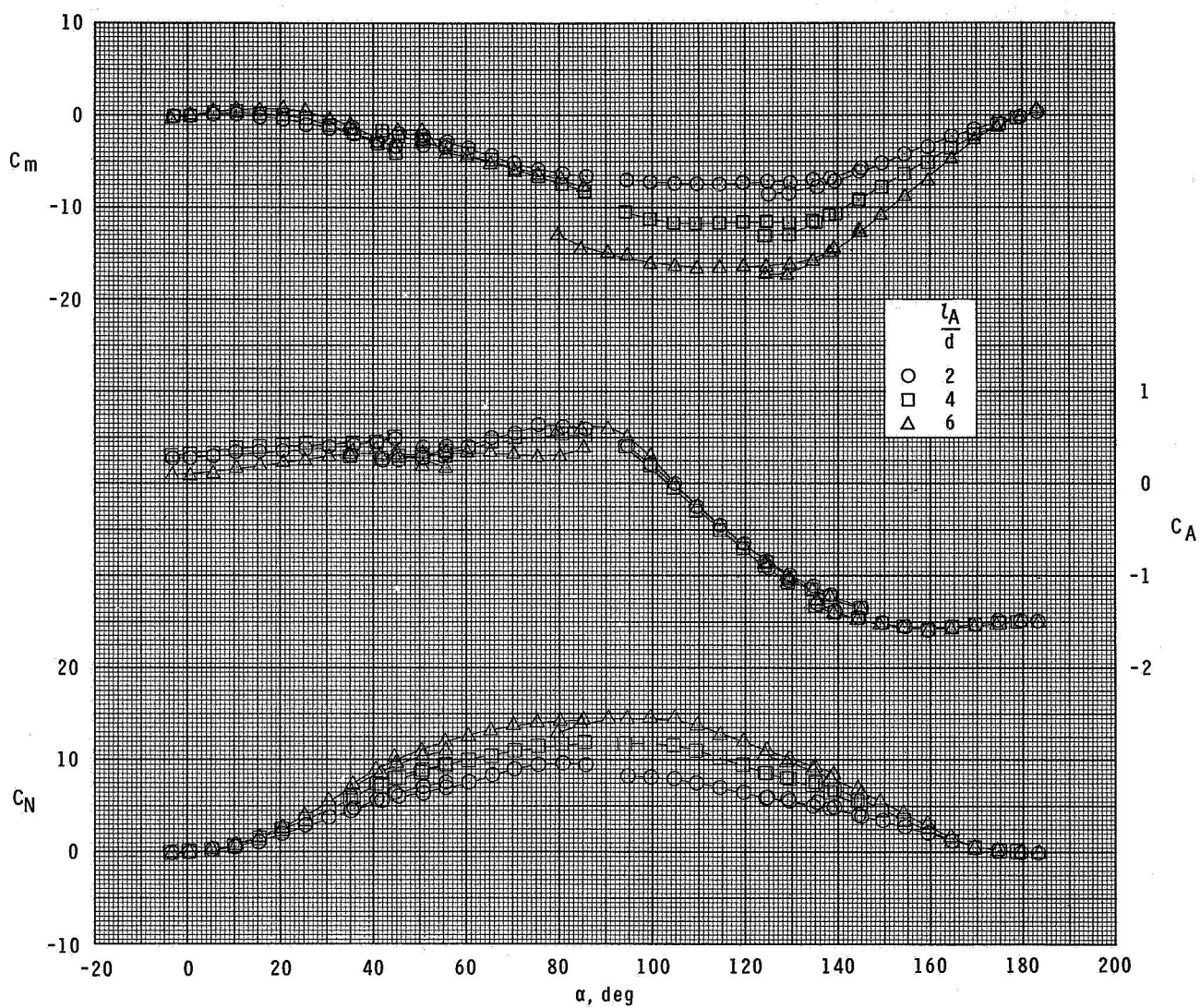
(c) $M = 2.36$.

Figure 4.- Continued.



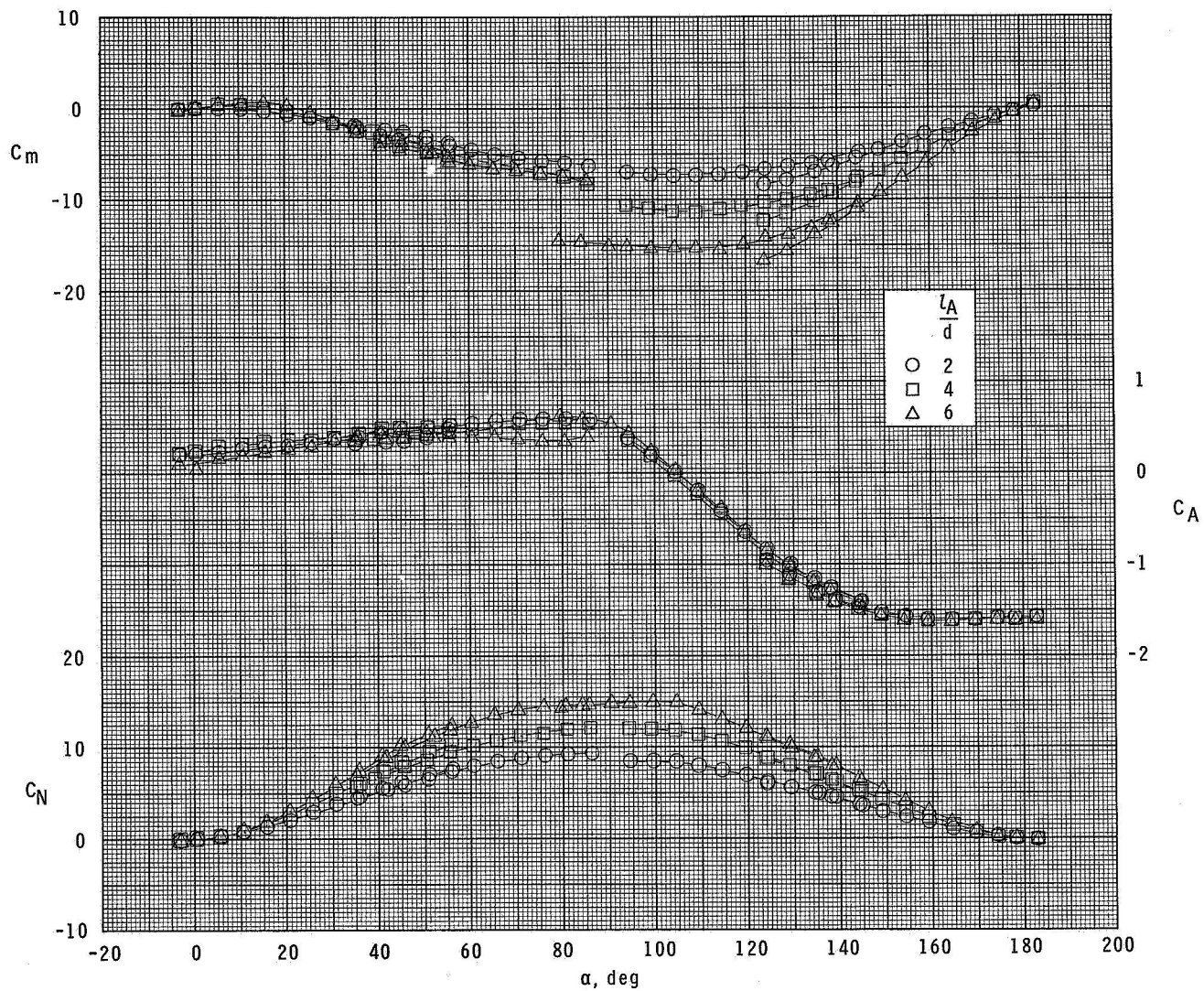
(d) $M=2.86$.

Figure 4.- Concluded.



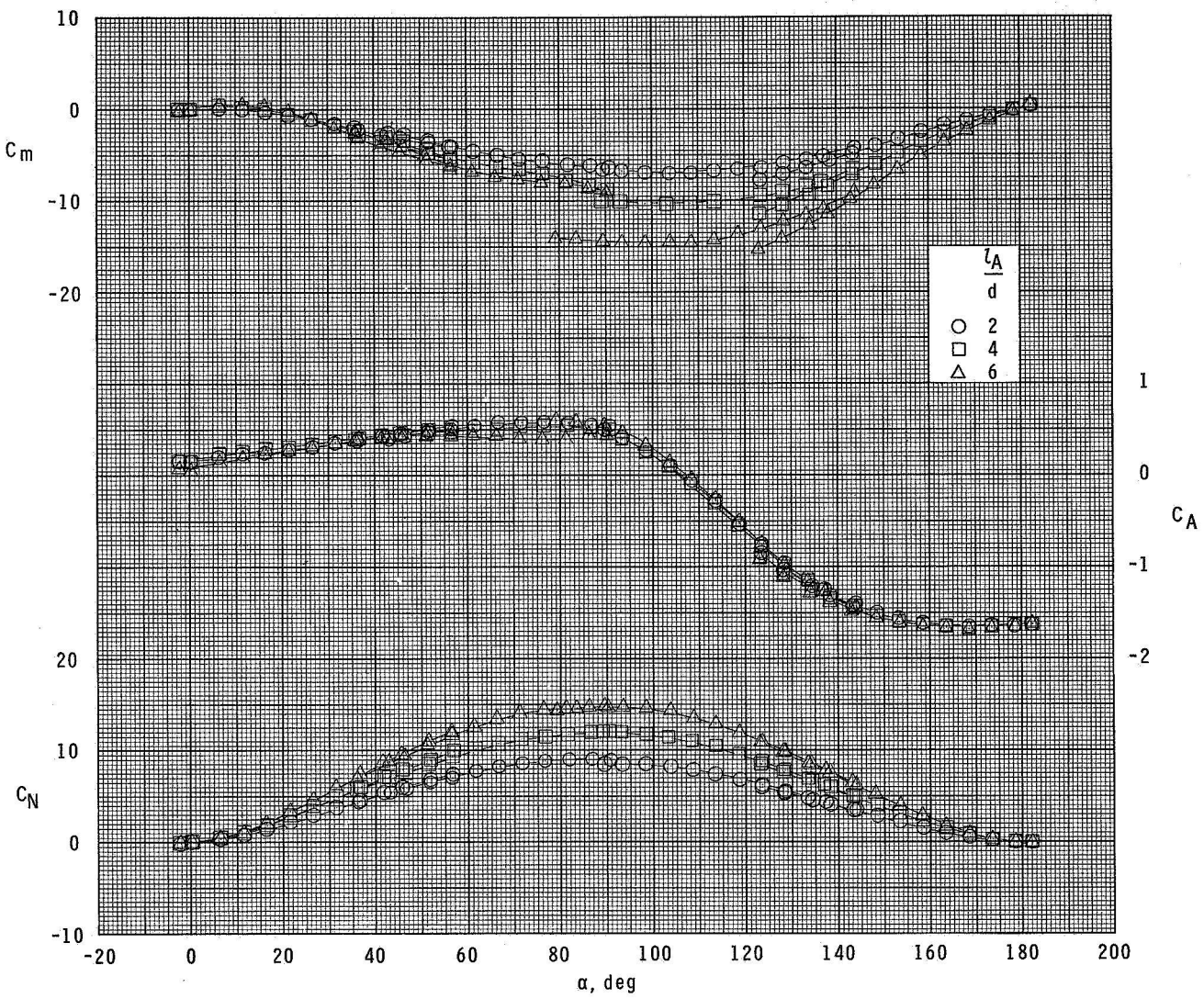
(a) $M=1.50$.

Figure 5.- Effect of afterbody fineness ratio on longitudinal stability characteristics of ogive-cylinder models with nose fineness ratio of 5.



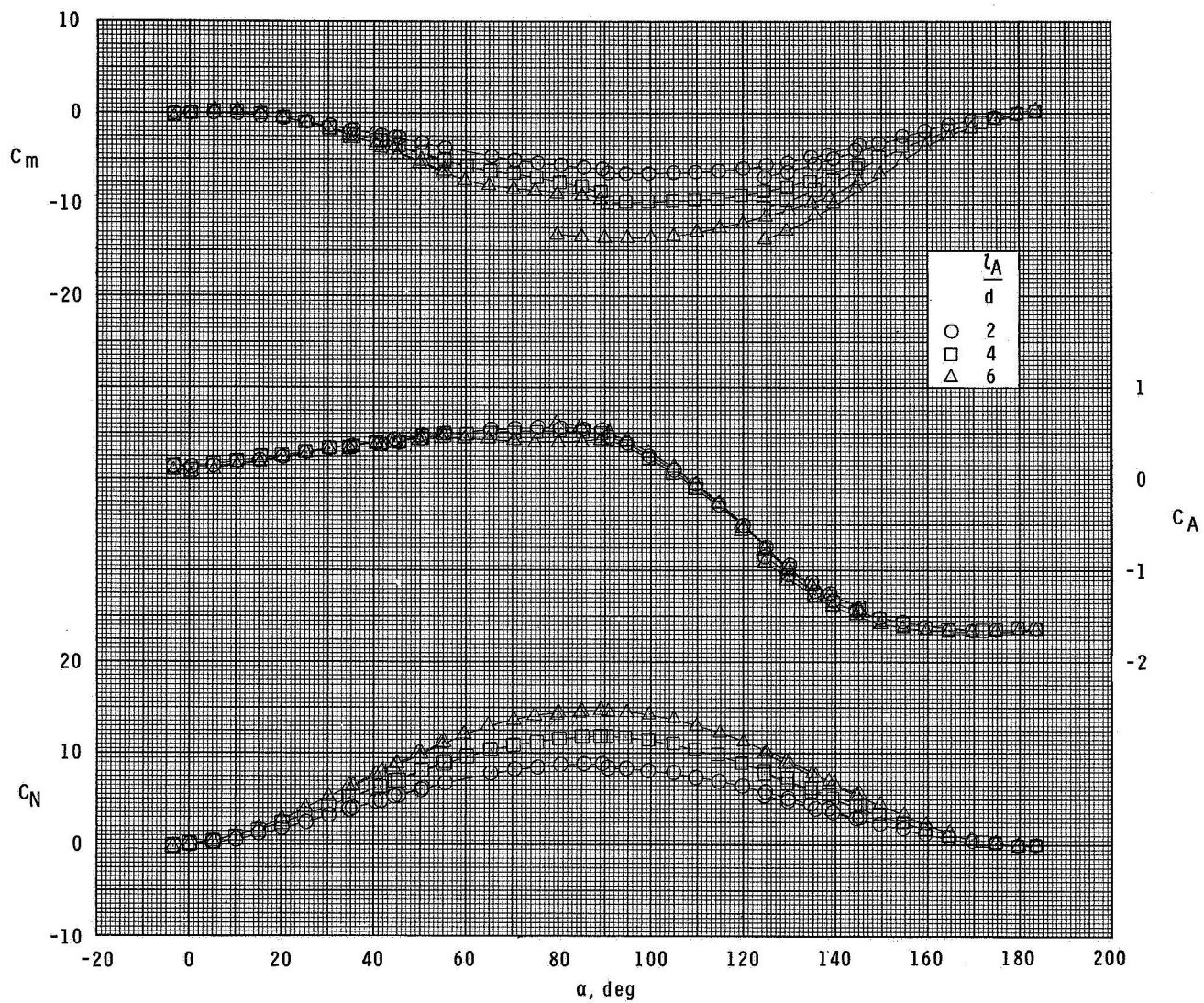
(b) $M = 1.90$.

Figure 5.- Continued.



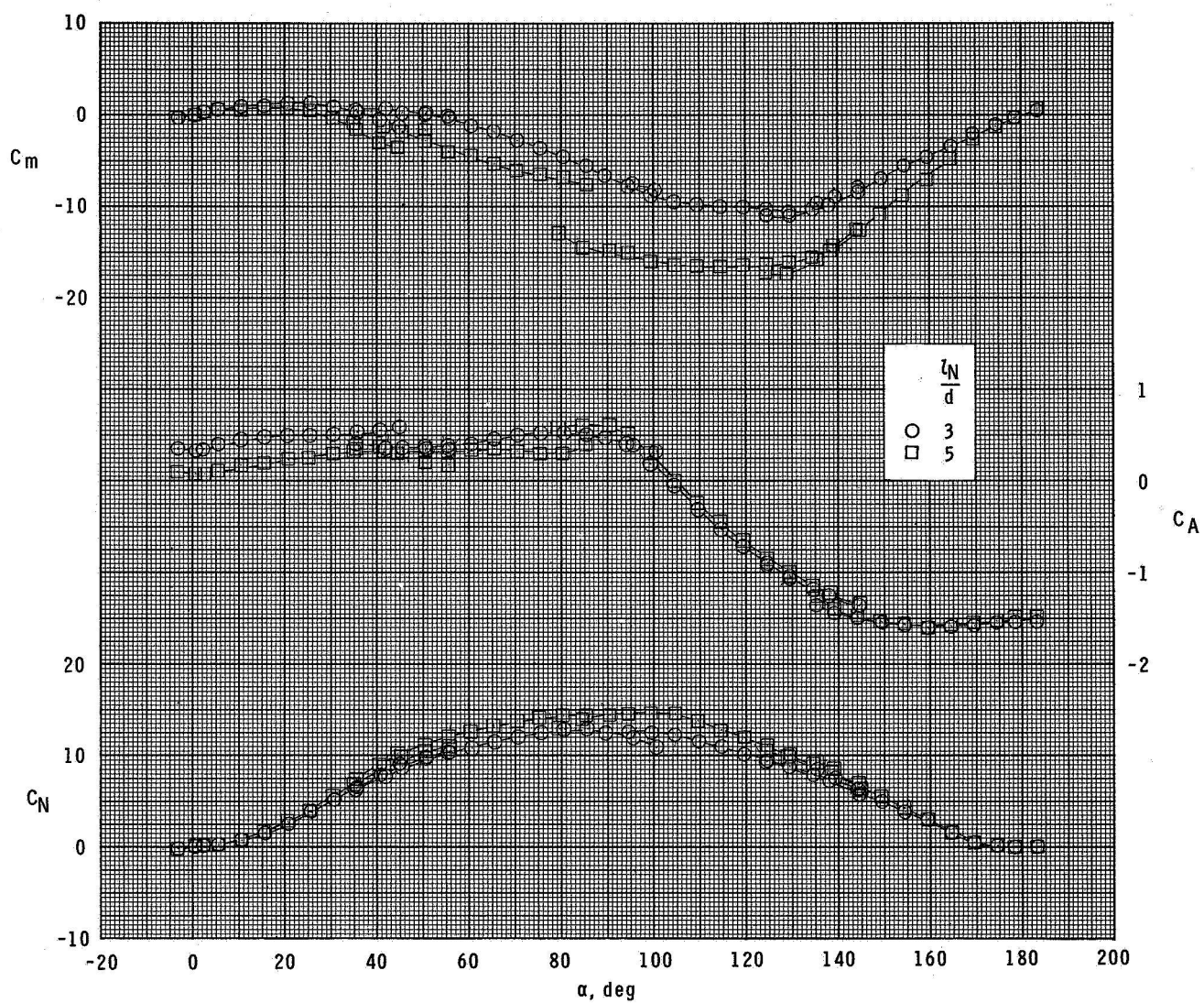
(c) $M=2.36$.

Figure 5.- Continued.



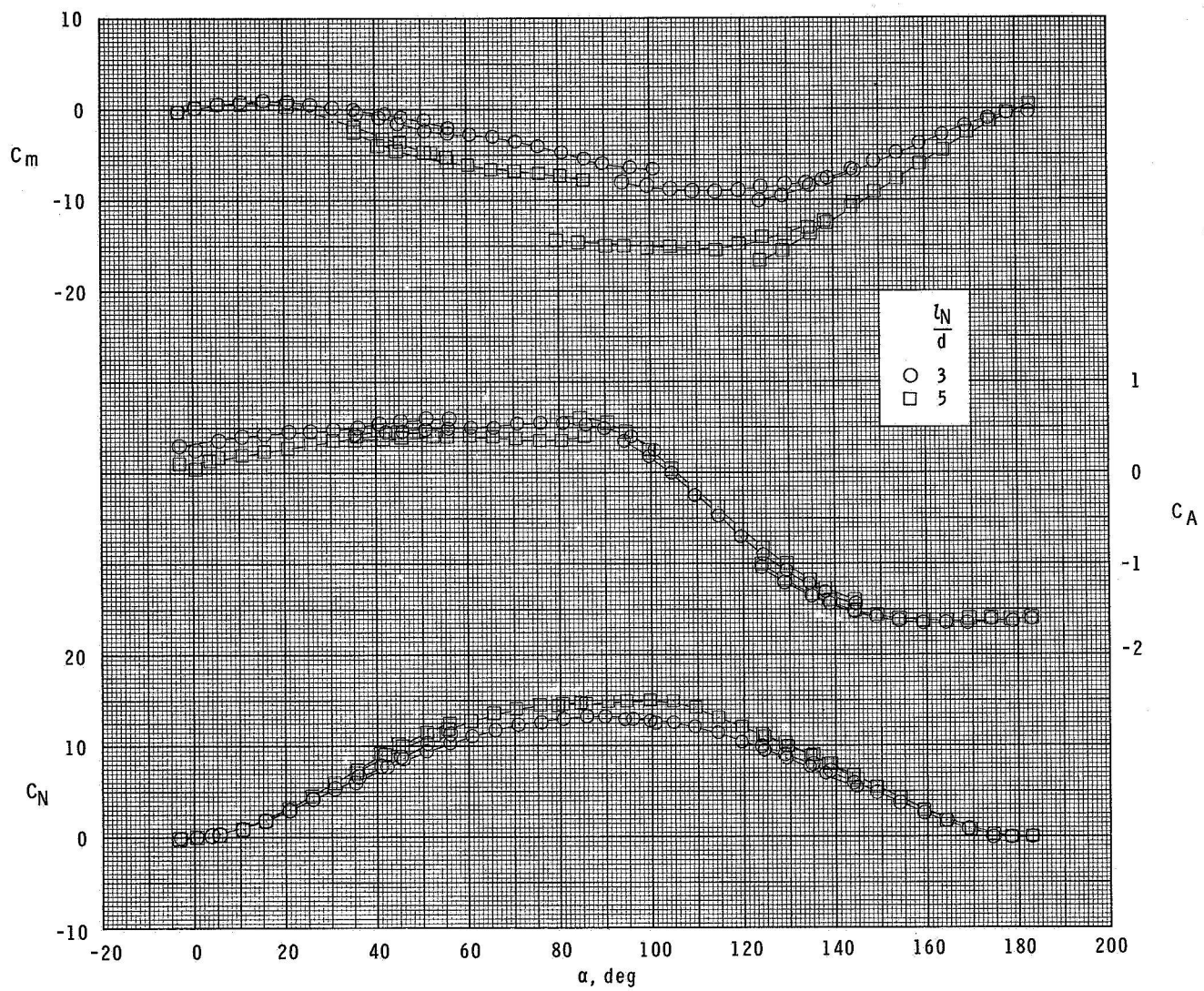
(d) $M=2.86$.

Figure 5.- Concluded.



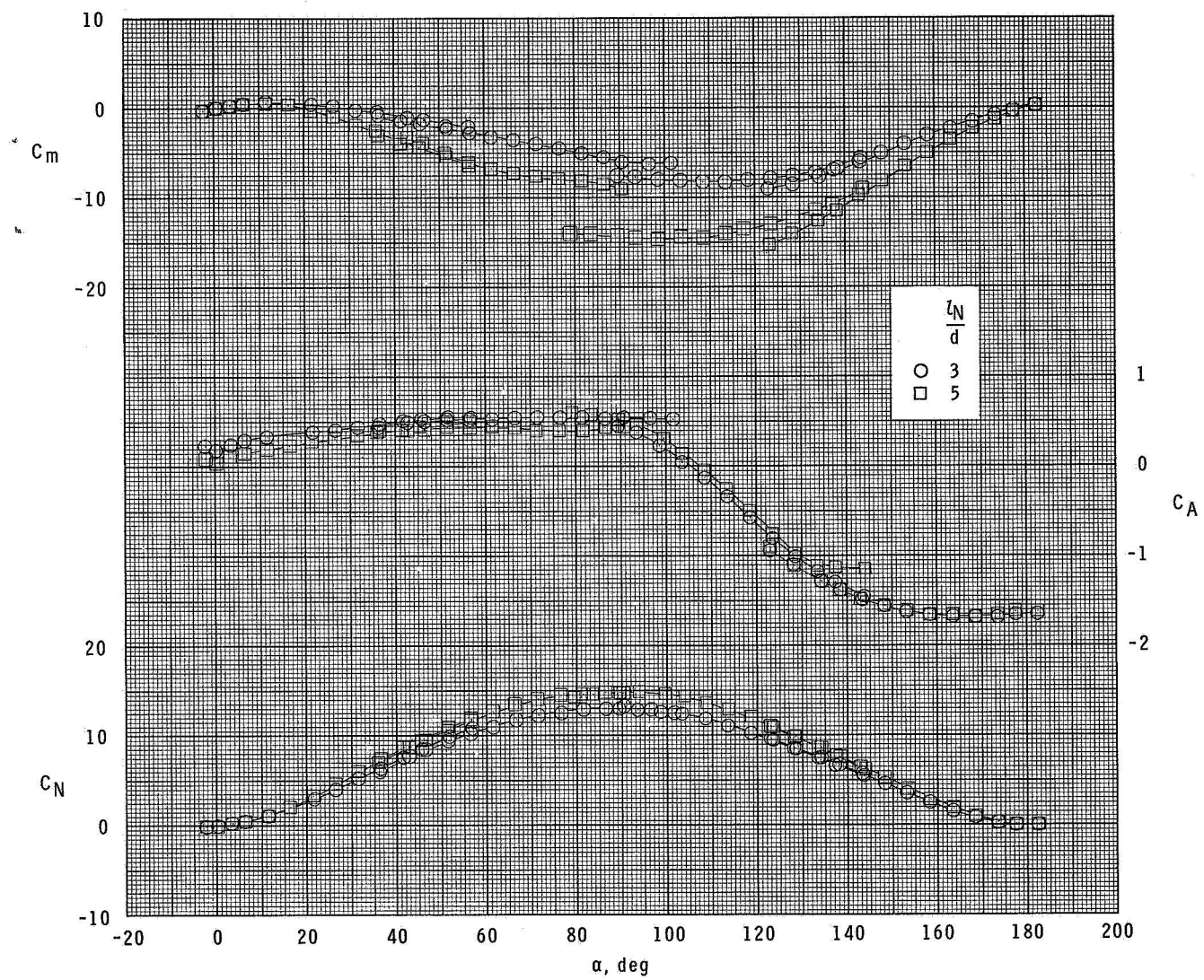
(a) $M = 1.50$.

Figure 6.- Effect of nose fineness ratio on longitudinal stability characteristics of ogive-cylinder models with afterbody fineness ratio of 6.



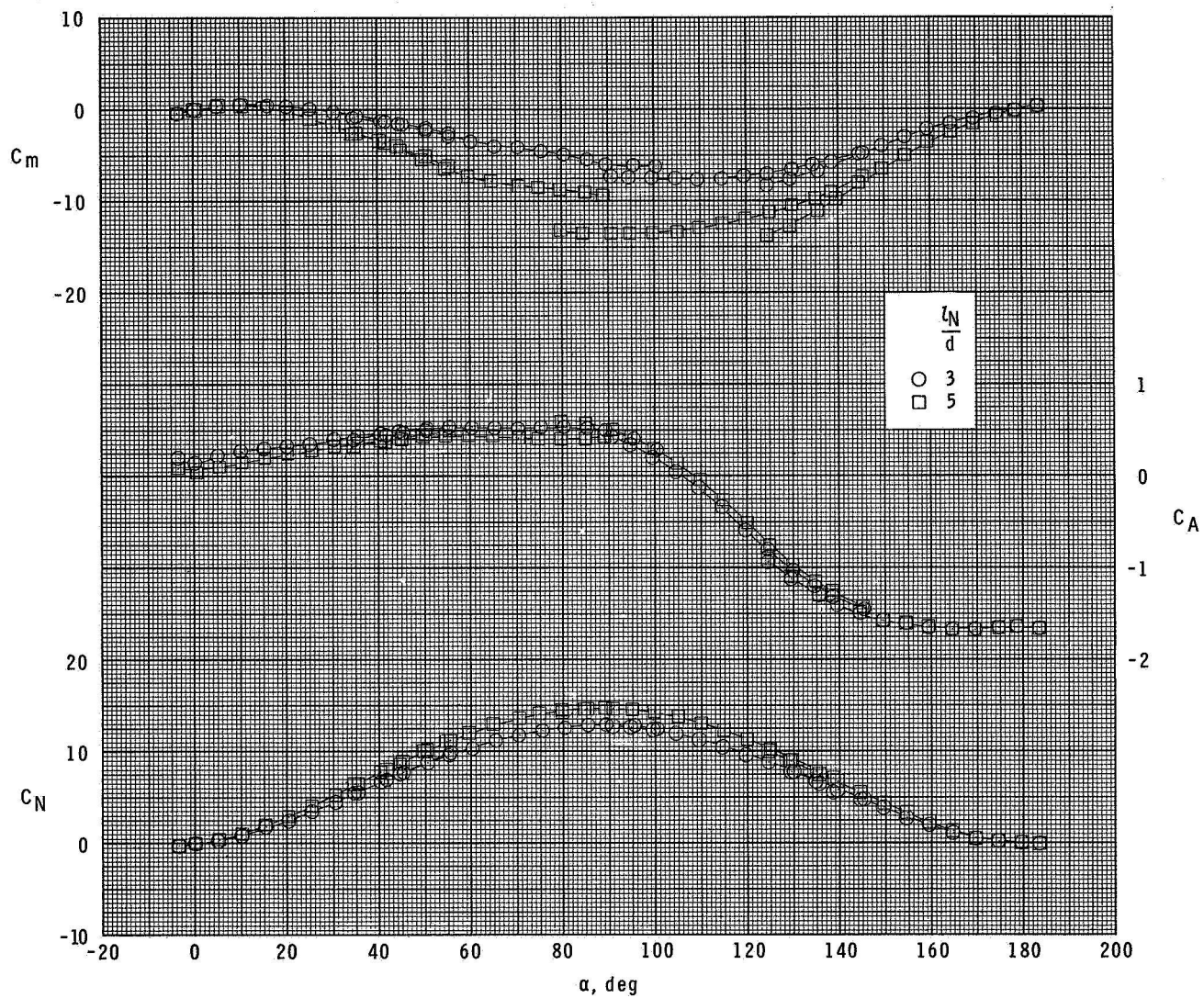
(b) $M=1.90$.

Figure 6.- Continued.



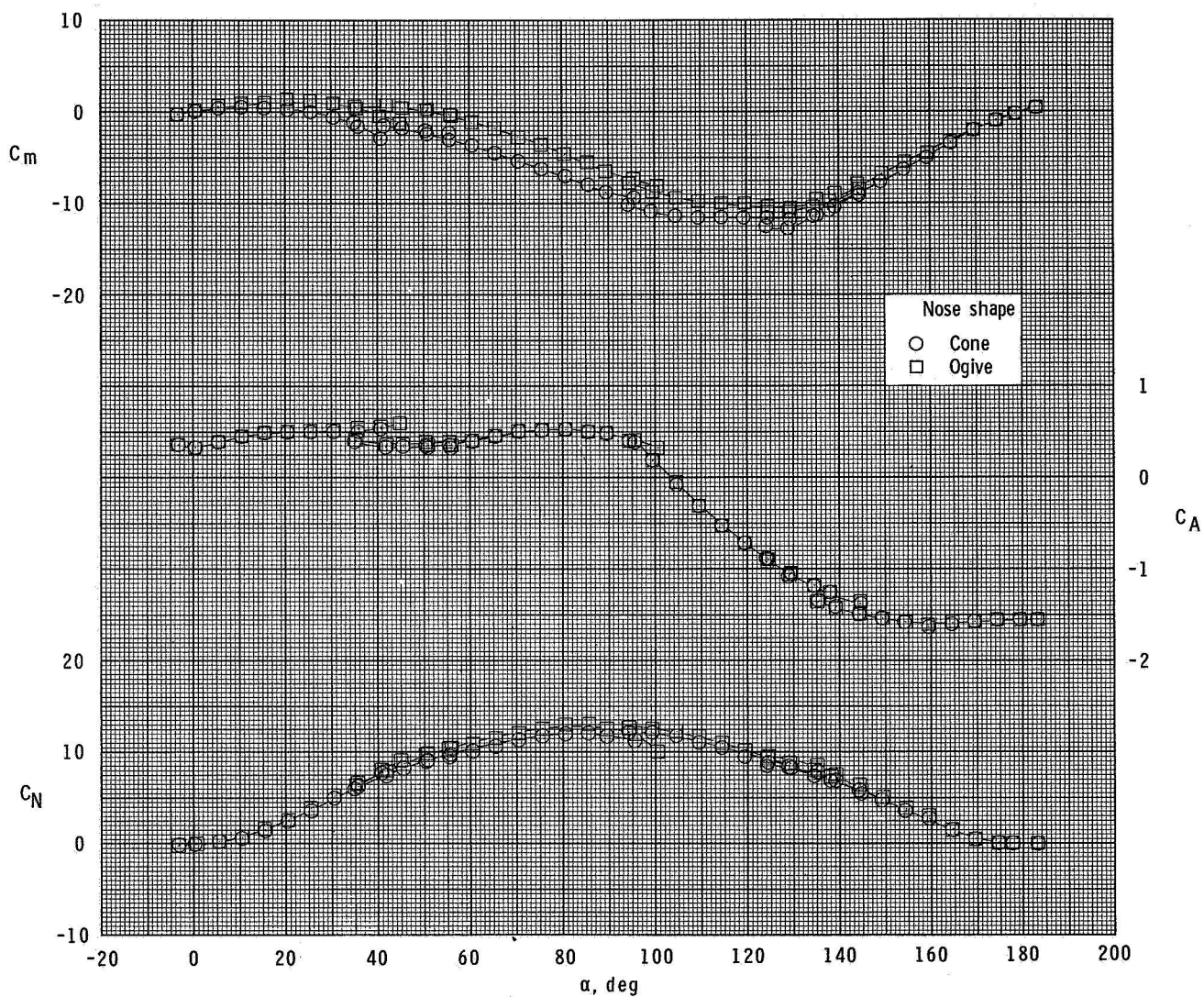
(c) $M=2.36$.

Figure 6.- Continued.



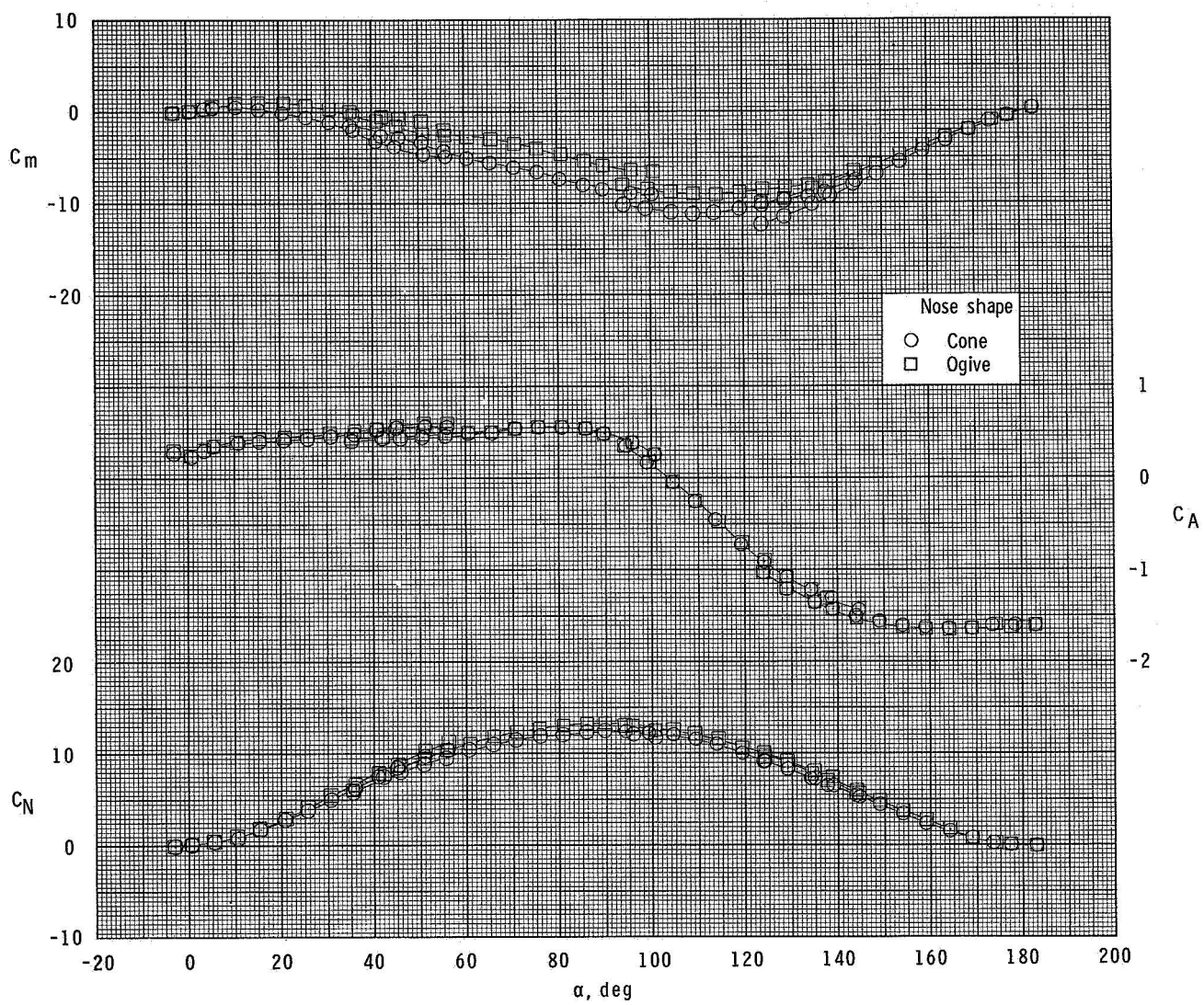
(d) $M = 2.86$.

Figure 6.- Concluded.



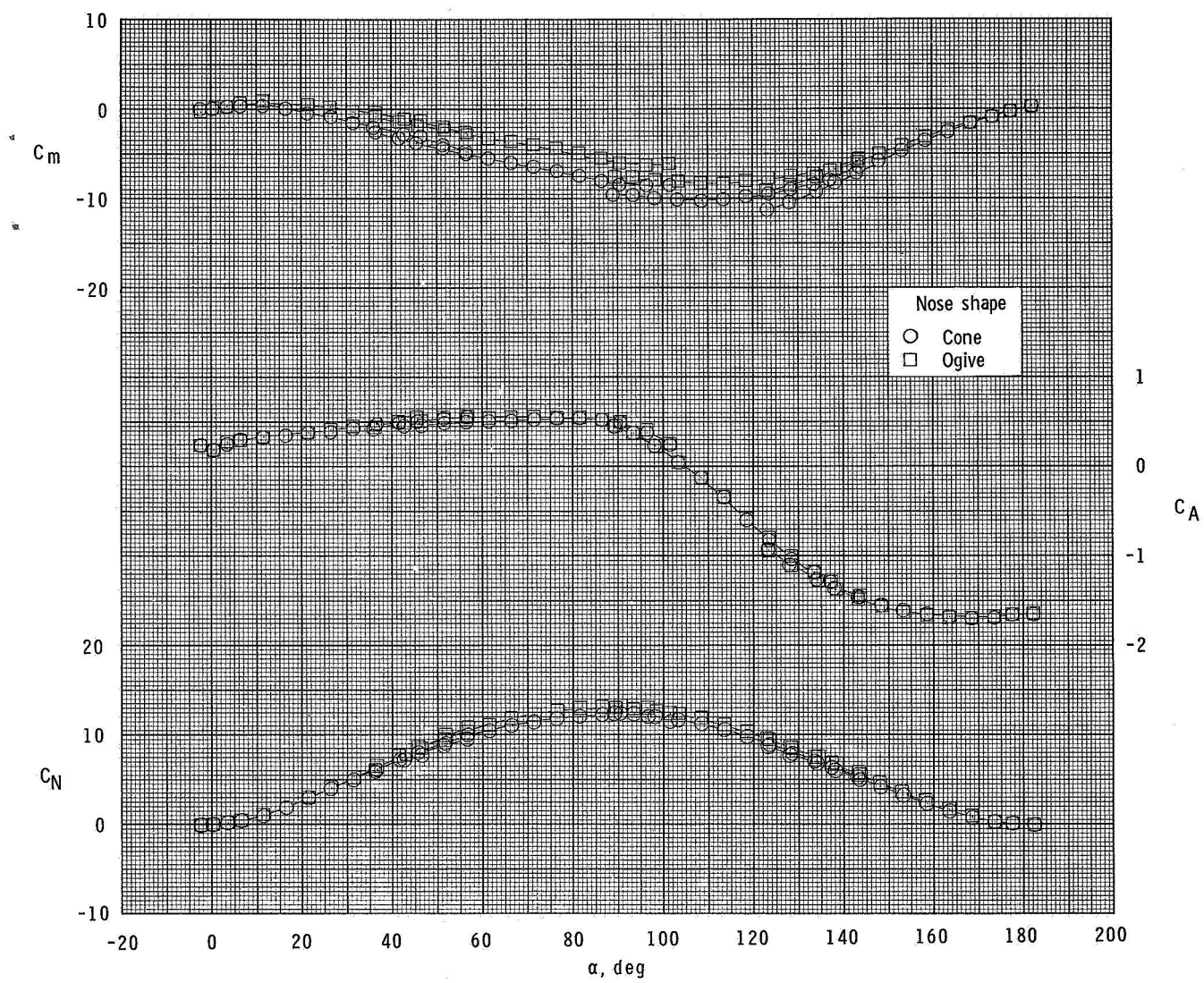
(a) $M = 1.50$.

Figure 7.- Effect of nose shape on longitudinal stability characteristics of models with nose fineness ratio of 3 and afterbody fineness ratio of 6.



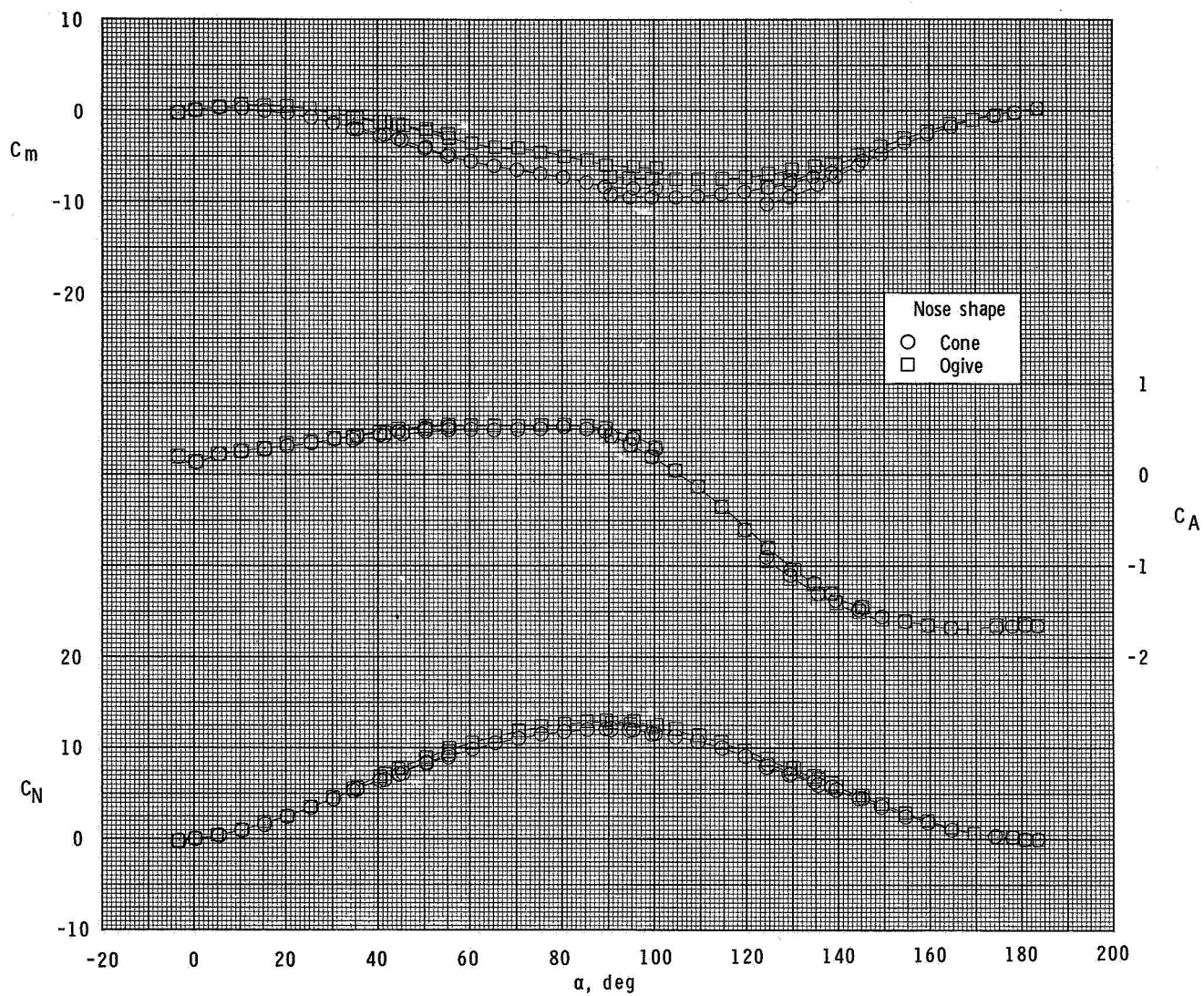
(b) $M=1.90$.

Figure 7.- Continued.



(c) $M=2.36$.

Figure 7.- Continued.



(d) $M=2.86$.

Figure 7.- Concluded.

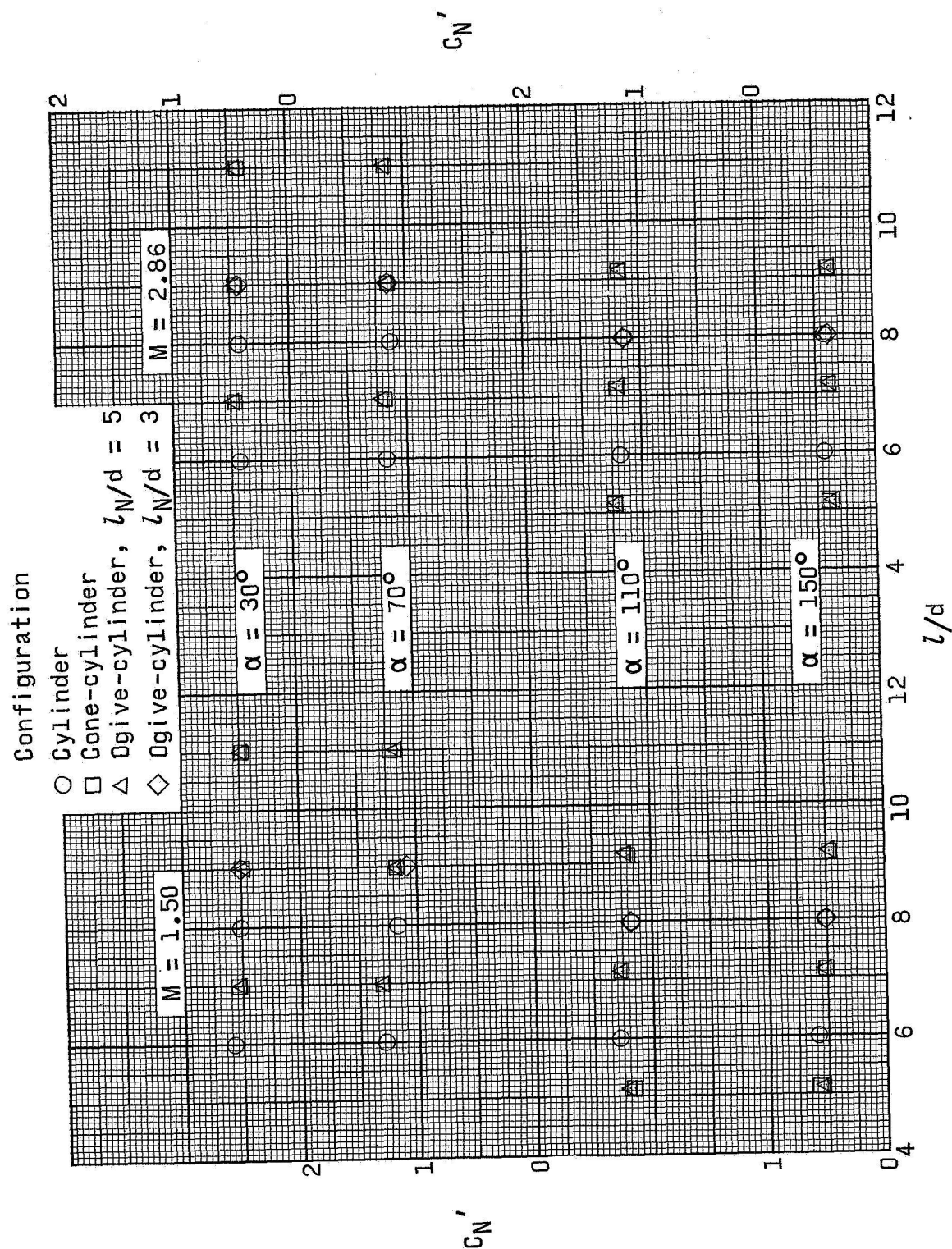
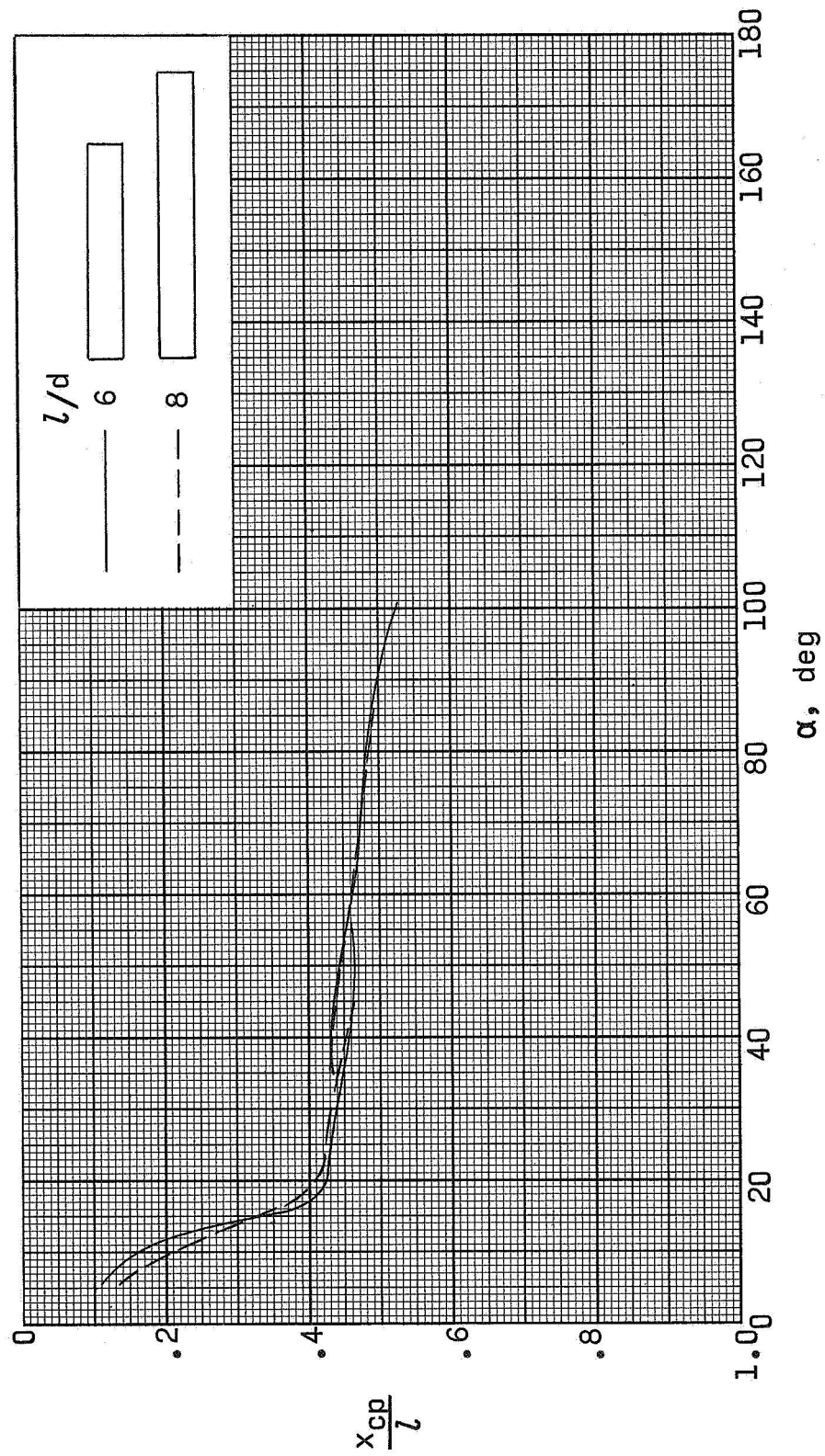
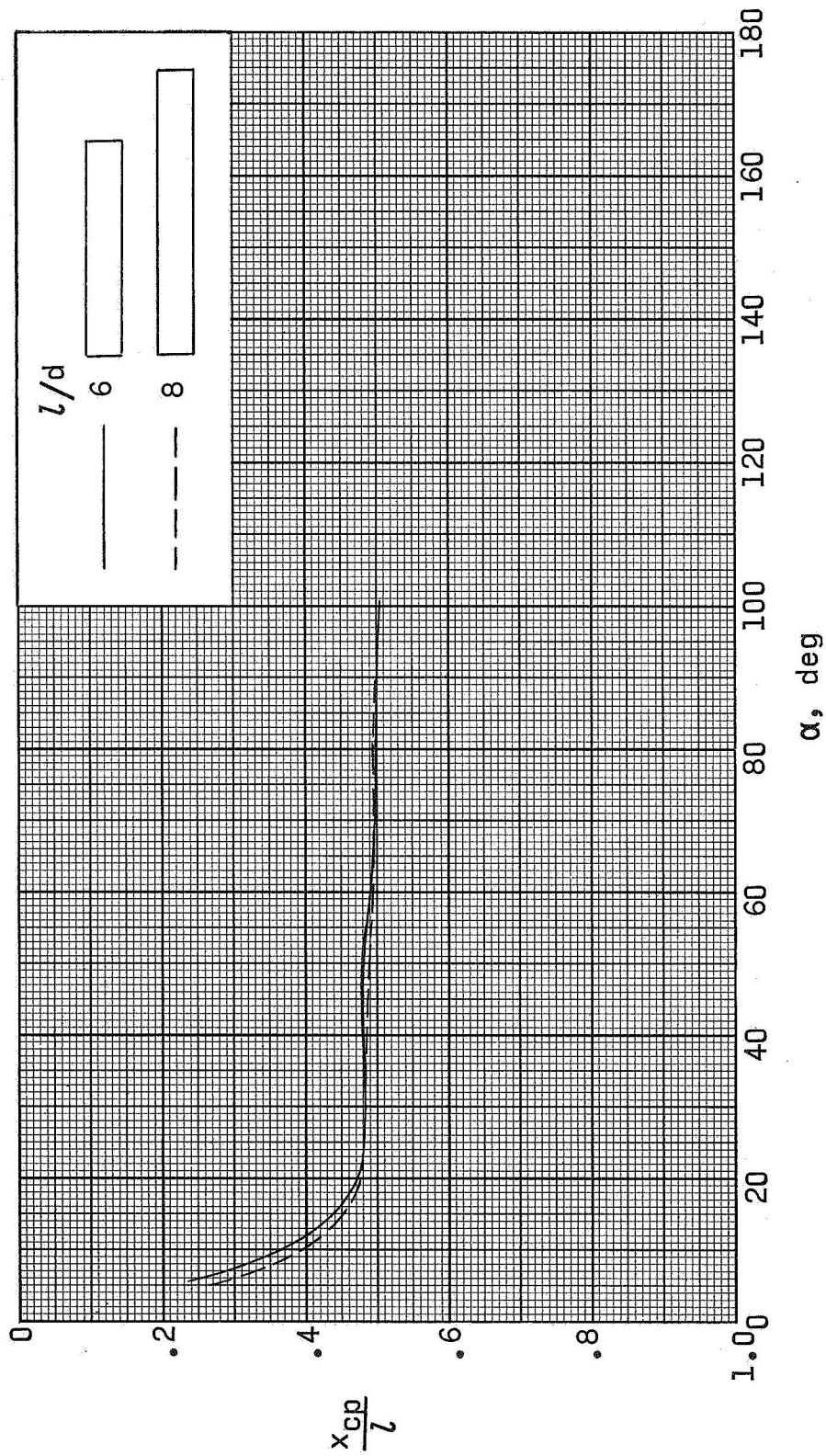


Figure 8.- Variation of normal-force coefficient based on planform area with fineness ratio.



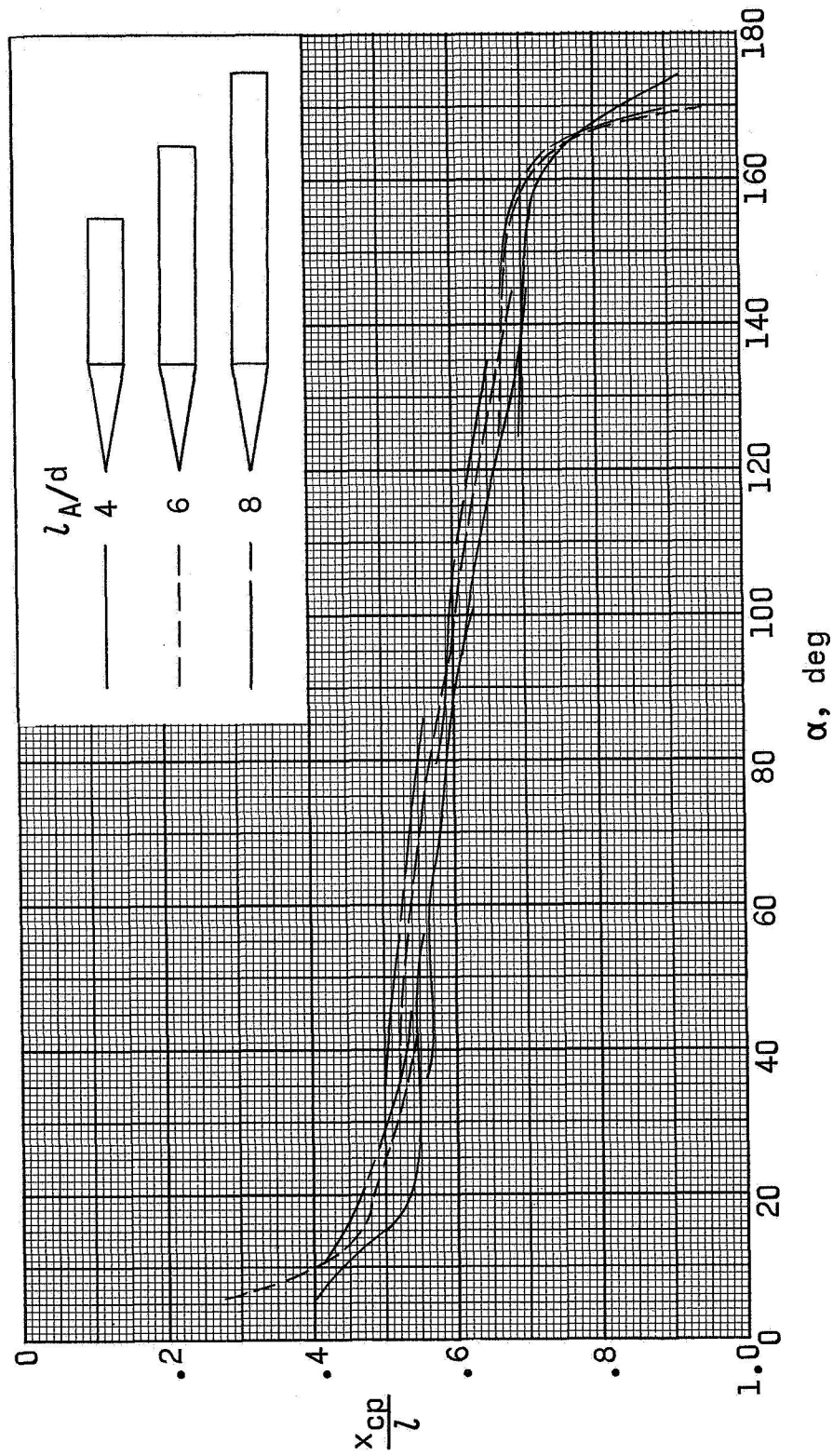
(a) $M = 1.50$.

Figure 9.- Effect of fineness ratio on center of pressure for cylindrical models.



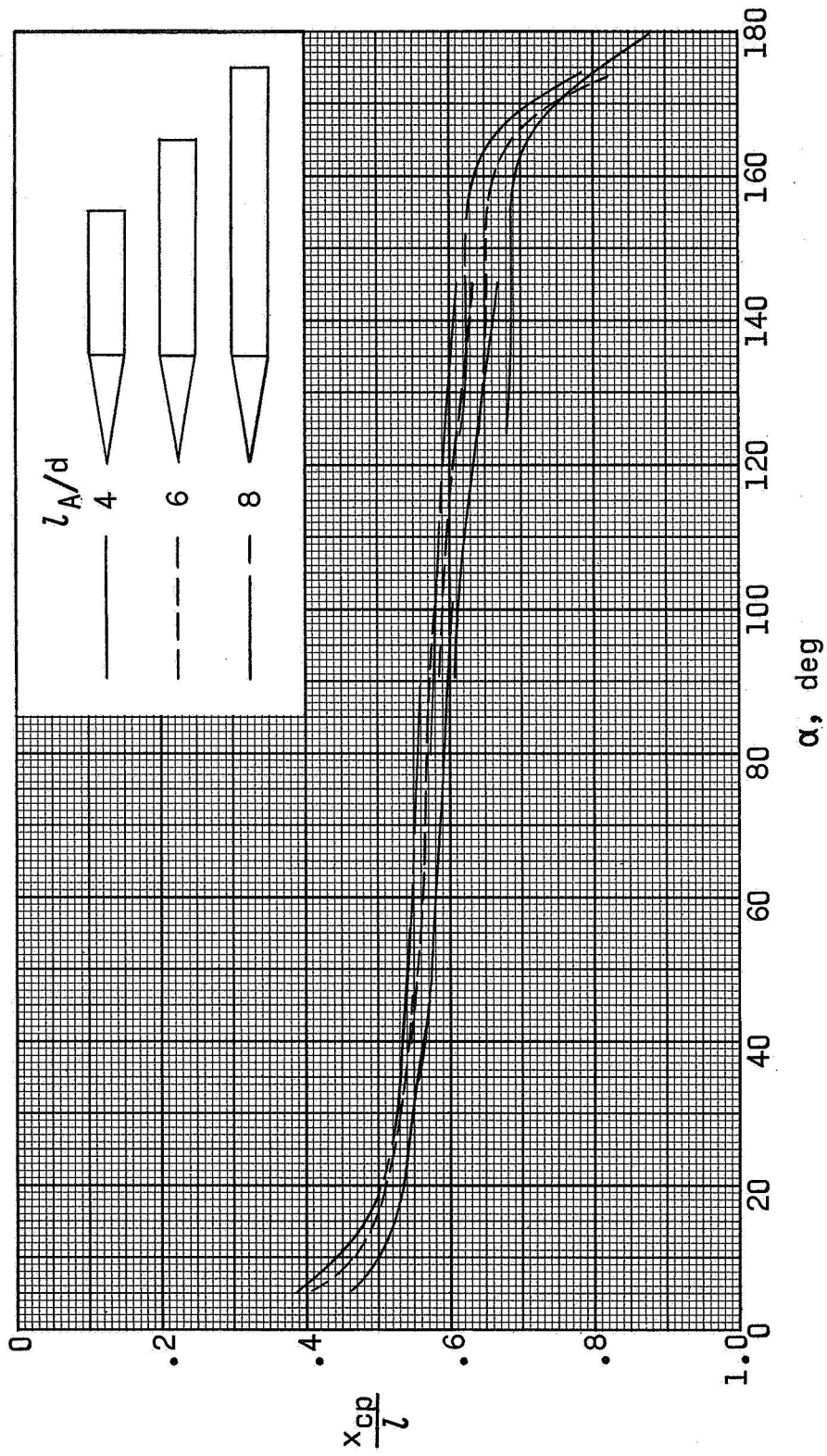
(b) $M = 2.86$.

Figure 9.- Concluded.



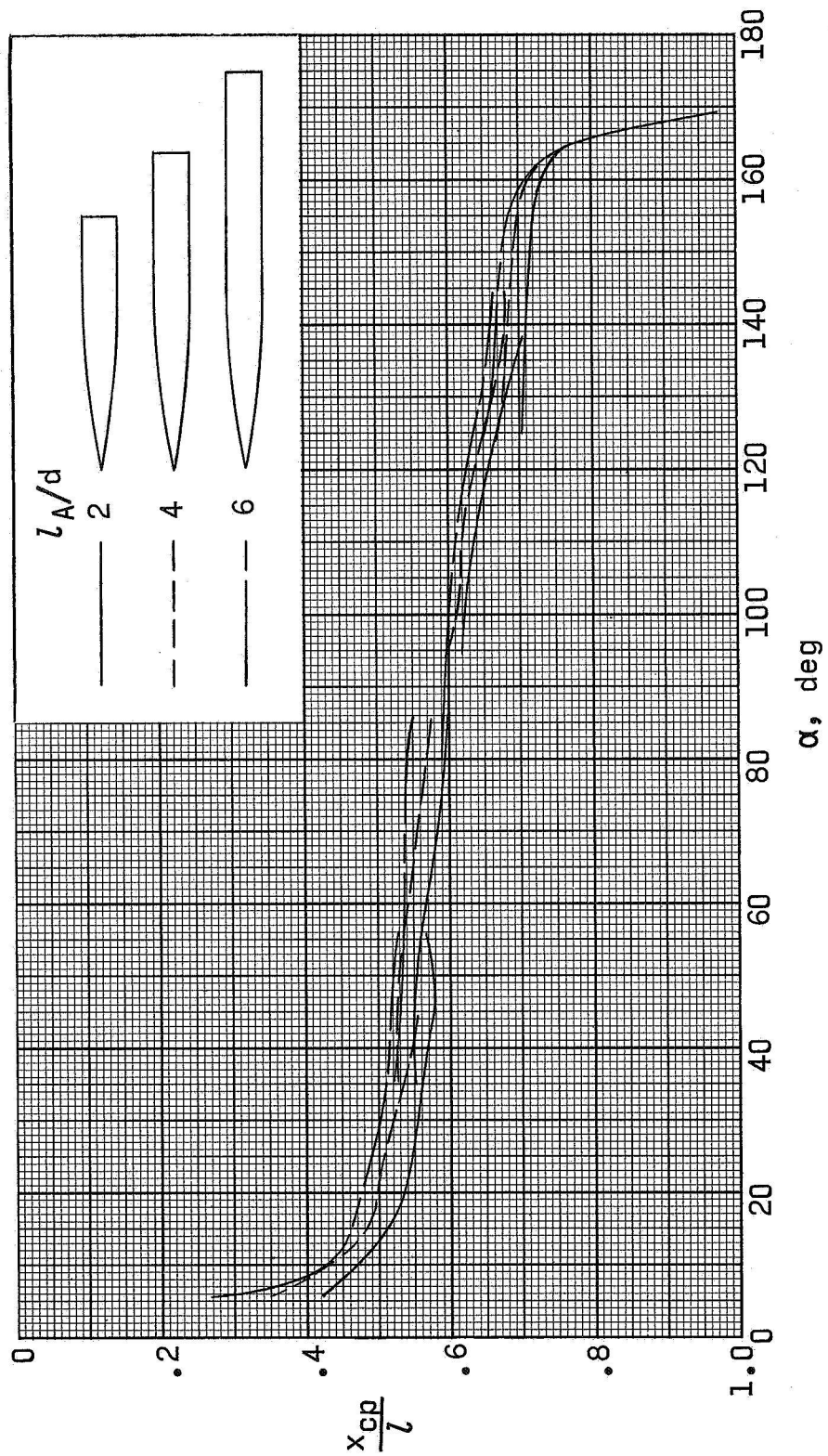
(a) $M = 1.50$.

Figure 10.- Effect of afterbody fineness ratio on center of pressure for cone-cylinder models with nose fineness ratio of 3.



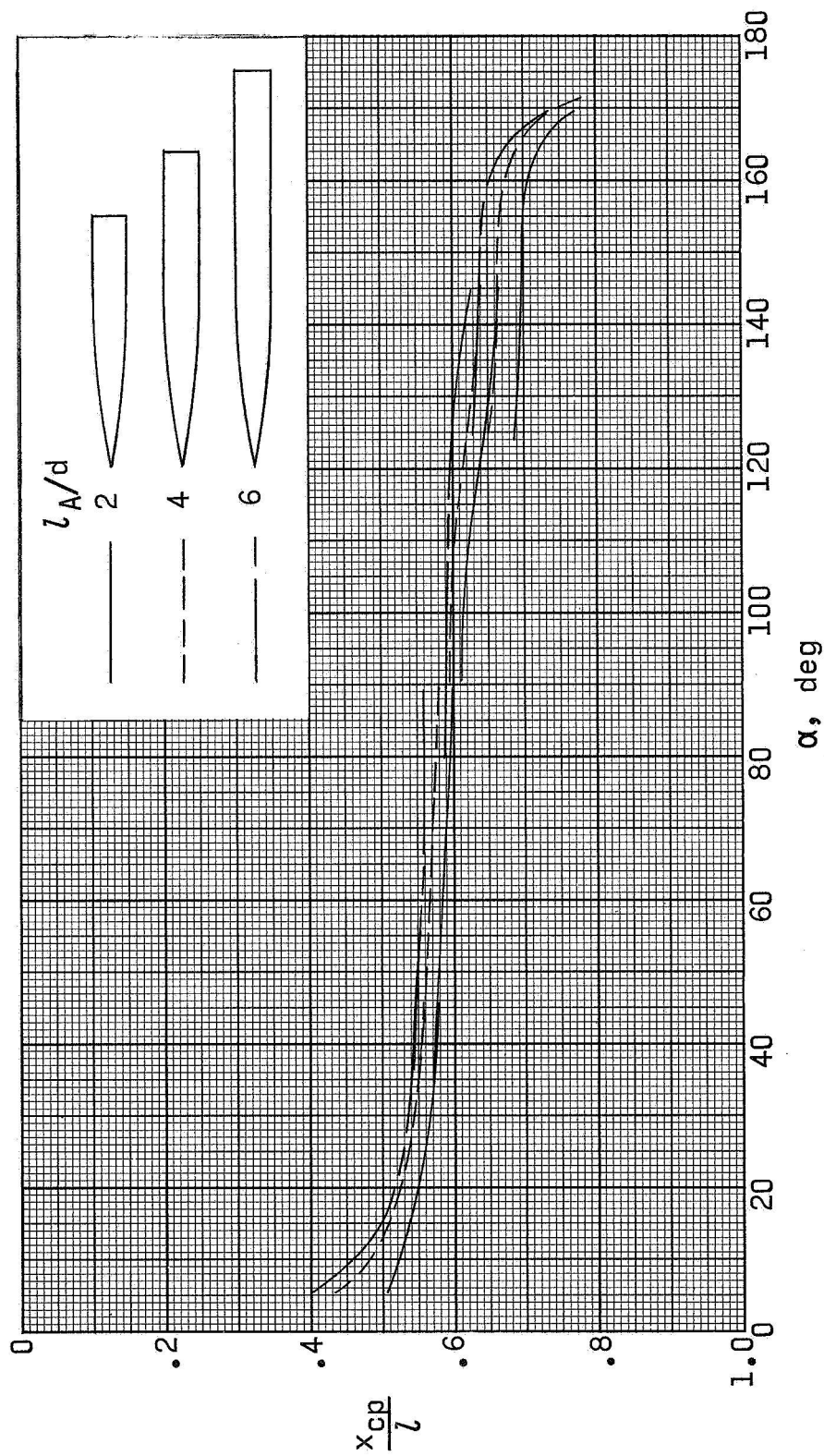
(b) $M = 2.86$.

Figure 10.- Concluded.



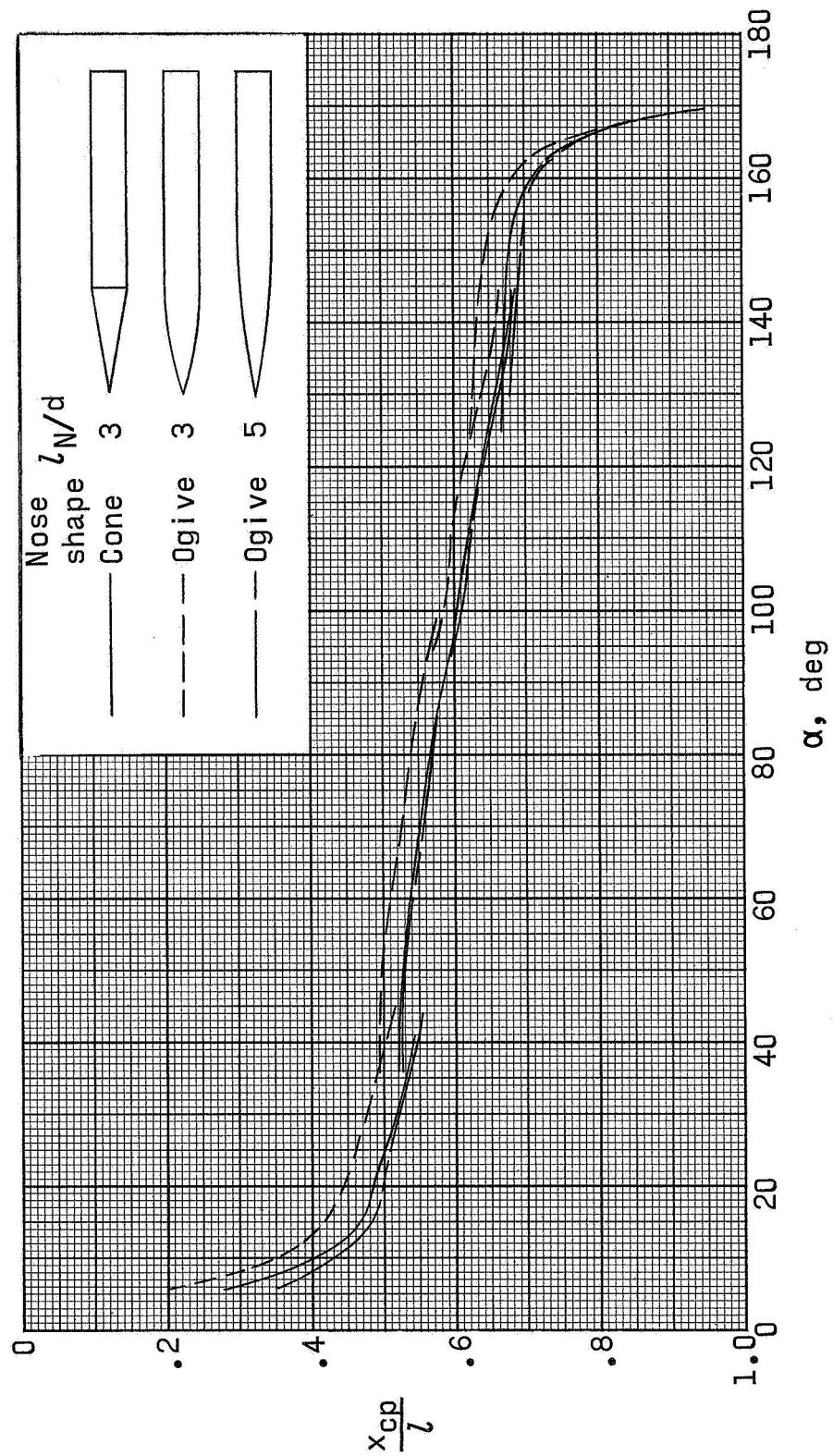
(a) $M = 1.50$.

Figure 11.- Effect of afterbody fineness ratio on center of pressure for ogive-cylinder models with nose fineness ratio of 5.



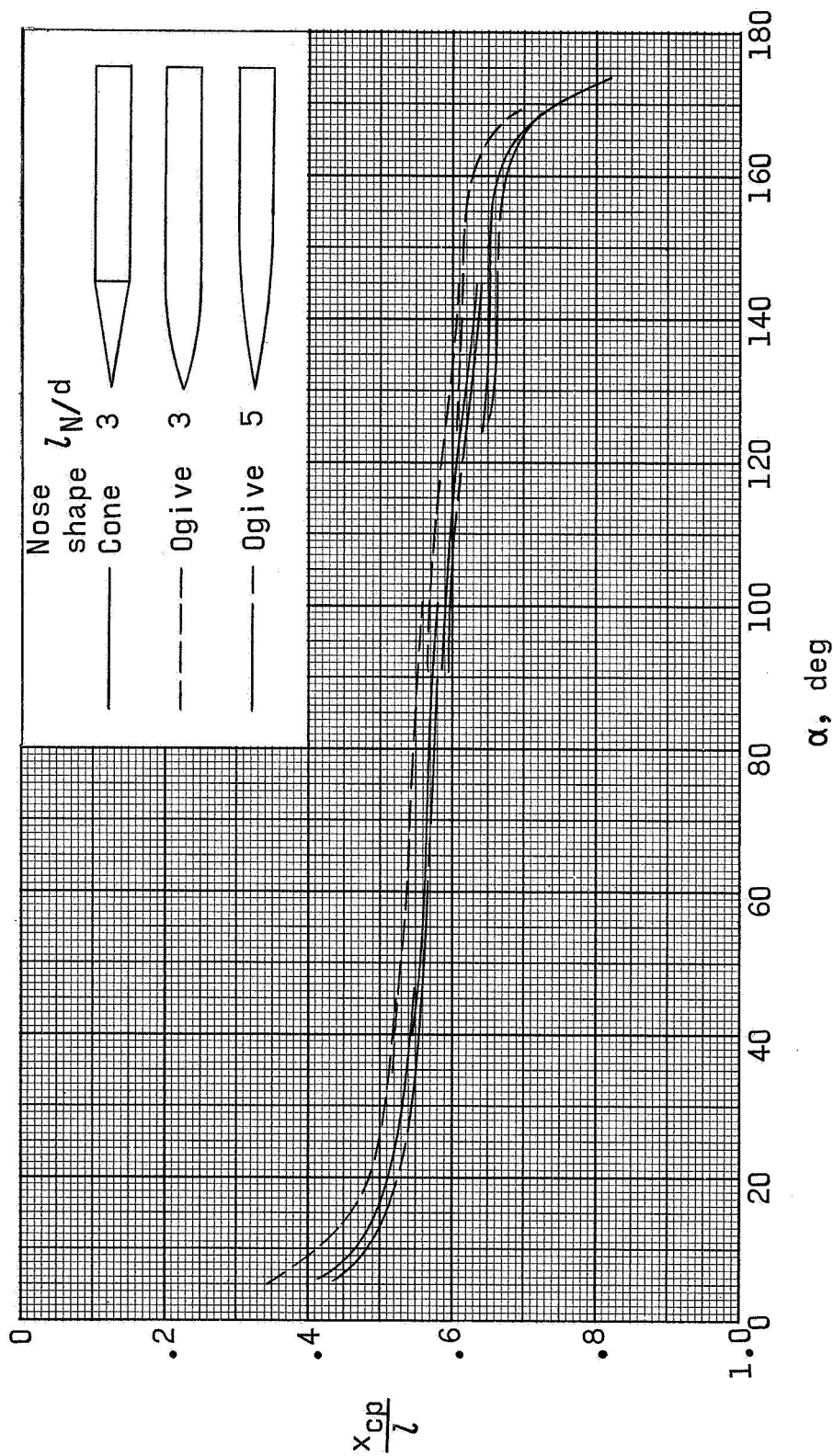
(b) $M = 2.86$.

Figure 11.- Concluded.



(a) $M = 1.50$.

Figure 12.- Effect of nose shape and nose fineness ratio on center of pressure for models with overall fineness ratio of 9.



(b) $M = 2.86$.

Figure 12.- Concluded.

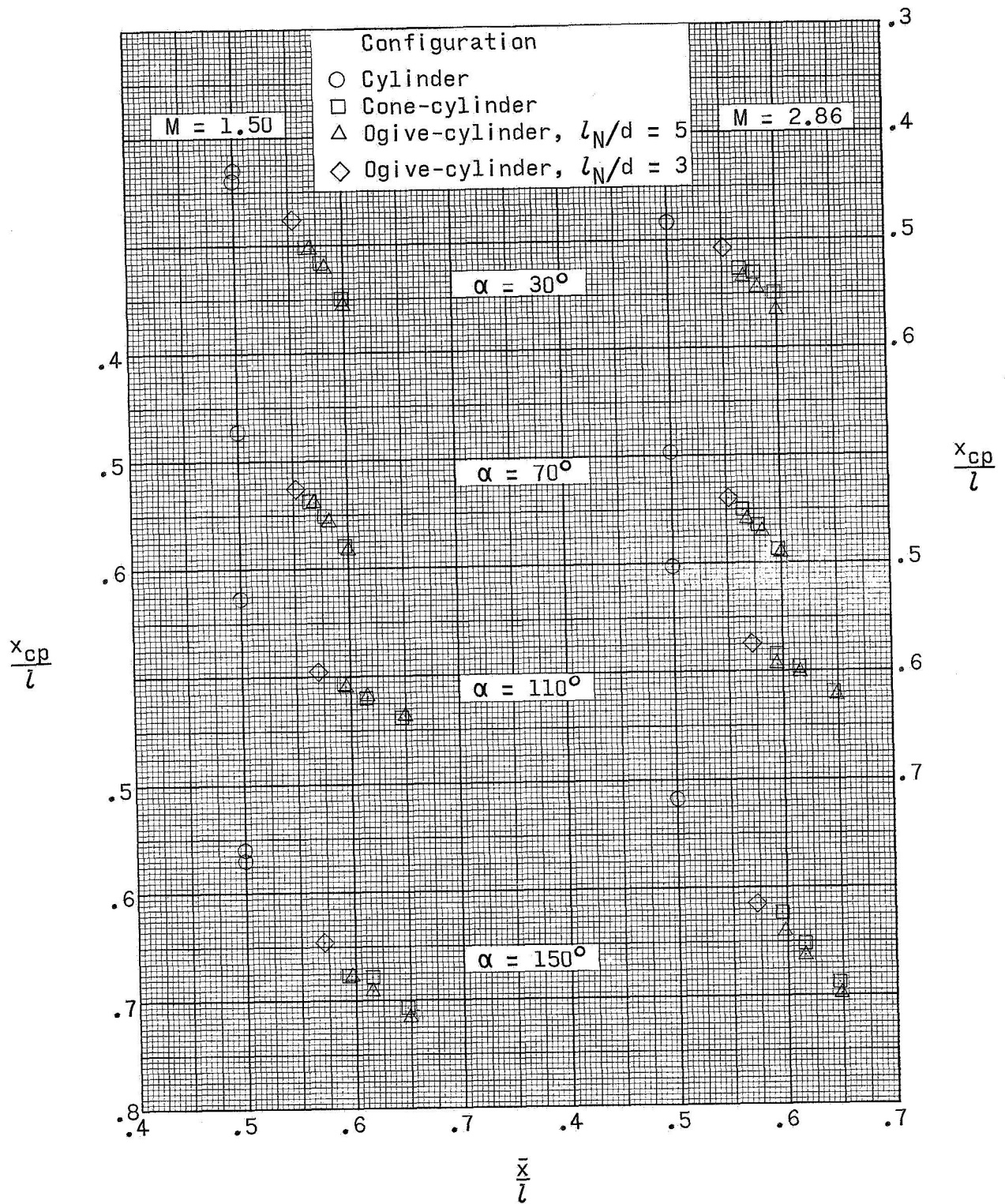


Figure 13.- Variation of center of pressure with planform-area centroid.

NATIONAL AERONAUTICS AND SPACE ADMINISTRATION
WASHINGTON, D. C. 20546
OFFICIAL BUSINESS

FIRST CLASS MAIL

POSTAGE AND FEES PAID
NATIONAL AERONAUTICS AND
SPACE ADMINISTRATION

POSTMASTER: If Undeliverable (Section 158,
Postal Manual) Do Not Return

"The aeronautical and space activities of the United States shall be conducted so as to contribute . . . to the expansion of human knowledge of phenomena in the atmosphere and space. The Administration shall provide for the widest practicable and appropriate dissemination of information concerning its activities and the results thereof."

— NATIONAL AERONAUTICS AND SPACE ACT OF 1958

NASA SCIENTIFIC AND TECHNICAL PUBLICATIONS

TECHNICAL REPORTS: Scientific and technical information considered important, complete, and a lasting contribution to existing knowledge.

TECHNICAL NOTES: Information less broad in scope but nevertheless of importance as a contribution to existing knowledge.

TECHNICAL MEMORANDUMS: Information receiving limited distribution because of preliminary data, security classification, or other reasons.

CONTRACTOR REPORTS: Scientific and technical information generated under a NASA contract or grant and considered an important contribution to existing knowledge.

TECHNICAL TRANSLATIONS: Information published in a foreign language considered to merit NASA distribution in English.

SPECIAL PUBLICATIONS: Information derived from or of value to NASA activities. Publications include conference proceedings, monographs, data compilations, handbooks, sourcebooks, and special bibliographies.

TECHNOLOGY UTILIZATION PUBLICATIONS: Information on technology used by NASA that may be of particular interest in commercial and other non-aerospace applications. Publications include Tech Briefs, Technology Utilization Reports and Notes, and Technology Surveys.

Details on the availability of these publications may be obtained from:

SCIENTIFIC AND TECHNICAL INFORMATION DIVISION
NATIONAL AERONAUTICS AND SPACE ADMINISTRATION
Washington, D.C. 20546